CMI

www.nature.com/cmi

ARTICLE

Dextran sodium sulfate potentiates NLRP3 inflammasome activation by modulating the KCa3.1 potassium channel in a mouse model of colitis

Bo Zeng[1,2], Yuanting Huang[2], Siyuan Chen[2], Rong Xu[2], Lihui Xu[3], Jiahao Qiu[2], Fuli Shi[2], Siying Liu[2], Qingbing Zha[1,4]✉, Dongyun Ouyang[2]✉ and Xianhui He[1,2]✉

Inflammatory bowel disease (IBD), including Crohn's disease and ulcerative colitis, has increased in incidence and prevalence in recent decades. Both clinical and animal studies are critical for understanding the pathogenesis of this disease. Dextran sodium sulfate (DSS)-induced colitis is a frequently used animal model of IBD, but the underlying mechanism of the model remains incompletely understood. In this study, we found that NOD-like receptor family pyrin containing 3 (NLRP3) depletion markedly mitigated DSS-induced colitis and was accompanied by decreased activation of the inflammasome in the colons of mice. However, in vitro assays showed that DSS did not directly trigger but instead potentiated NLRP3 inflammasome assembly in macrophages in response to suboptimal ATP or nigericin stimulation. Mechanistically, DSS potentiated NLRP3 inflammasome activation in macrophages by augmenting KCa3.1-mediated potassium ion (K^+) efflux. Furthermore, we found that pharmacologic blockade of the K^+ channel KCa3.1 with TRAM-34 or genetic depletion of the *Kcnn4* gene (encoding KCa3.1) not only ameliorated the severity of DSS-induced colitis but also attenuated in vivo inflammasome assembly in the colonic tissues of mice, suggesting a causal link between KCa3.1-mediated augmentation of the NLRP3 inflammasome and DSS-induced inflammatory injuries. Collectively, these results indicate that KCa3.1 plays a critical role in mediating DSS-induced colitis in mice by potentiating NLRP3 inflammasome activation. Our data provide a previously unknown mechanism by which DSS induces colitis in mice and suggests that KCa3.1 is an alternative therapeutic target for treating IBD.

Keywords: Inflammatory bowel disease; Inflammasome; Dextran sodium sulfate; Potassium ion channel; KCa3.1; TRAM-34.

Cellular & Molecular Immunology (2022) 19:925–943; https://doi.org/10.1038/s41423-022-00891-0

INTRODUCTION

Inflammatory bowel disease (IBD), including Crohn's disease and ulcerative colitis (UC), is characterized by chronic and relapsing inflammatory conditions affecting the gastrointestinal tract [1]. The incidence and prevalence of IBD have increased worldwide in recent decades [2]. Millions of people suffering from IBD are afflicted with recurrent diarrhea, rectal bleeding, abdominal pain, bowel obstruction, and other extraintestinal manifestations. Unfortunately, only approximately half of patients benefit from the currently available medical treatments, and a substantial proportion of patients still require colectomy [3]. For those initial responders, the loss of responses over time, systemic immunosuppression, increased risk of cancer, infections, and other well-described adverse effects are still inevitable [4]. Although the precise etiology of IBD remains unclear, the current consensus is that genetic factors synergistically act with environmental factors to promote disease occurrence and progression [5–7]. Recently, many proteins associated with immune signaling cascades have been shown to be involved in the dysregulated immune responses in IBD, but their precise roles remain to be further examined [1, 2]. Uncovering new targets, as well as their underlying mechanisms of action, by clinical investigations and preclinical animal model studies are therefore imperative for developing novel therapies to satisfy the unmet demands of IBD treatment.

In recent decades, animal models of IBD have been widely used to investigate the pathological processes and therapeutic strategies of IBD in preclinical studies. Over 40 animal models mimicking the clinical features of IBD have been established [8]. Among them, dextran sodium sulfate (DSS)-induced colitis is the most widely used model due to its many similarities to the key features of human UC symptoms and its ease of setup [8–10]. This model has also been frequently used to study the roles of innate immunity in IBD and to evaluate the pharmacodynamics of novel anti-inflammatory drugs because the adaptive immune system is not required for DSS-induced colitis [8].

[1]Department of Clinical Laboratory, The Fifth Affiliated Hospital of Jinan University, Heyuan, China. [2]Department of Immunobiology, College of Life Science and Technology, Jinan University, Guangzhou, China. [3]Department of Cell Biology, College of Life Science and Technology, Jinan University, Guangzhou, China. [4]Department of Fetal Medicine, The First Affiliated Hospital of Jinan University, Guangzhou, China. ✉email: zhaqingbb@sina.com; dongyun1967@aliyun.com; thexh@jnu.edu.cn

Received: 7 January 2022 Accepted: 6 June 2022
Published online: 7 July 2022

Although the precise mechanism(s) of action of DSS-induced colitis remain incompletely understood, it is generally believed that DSS exposure disrupts the intestinal epithelial barrier in animals, thereby exposing the cells in lamina propria (LP) to intestinal commensal bacteria, which leads to robust inflammatory responses and ultimately colitis [10]. A number of studies have revealed that innate immune cells, including neutrophils, monocytes and macrophages, play critical roles in mediating DSS-induced inflammatory responses [11]. Consistently, recent clinical studies showed that dysregulated innate immunity is associated with pediatric-onset colitis and IBD [12]. In innate immune cells, inflammasomes are important first lines of defense against pathogenic infections. Inflammasomes are cytosolic multiprotein complexes composed of distinct sensors, ASC, and pro-caspase-1, and their assembly is initiated by the detection of pathogen-associated molecular patterns (PAMPs), damage-associated molecular patterns (DAMPs) and/or sterile stressors [13]. Once assembled, pro-caspase-1 is recruited, autocatalytically activated and in turn processes pro-interleukin-1β (pro-IL-1β) and pro-IL-18 into mature IL-1β and IL-18, respectively, and initiates proinflammatory pyroptosis [13]. Many inflammasome-initiating sensors have been discovered [14]. Among these sensors, NOD-like receptor family pyrin containing 3 (NLRP3) is the most well-characterized due to its important roles in protecting against microbial infection and maintaining tissue homeostasis and because its overactivation is pathogenically involved in various human diseases, including gout, septic shock, atherosclerosis, and several autoimmune diseases [15–17]. Notably, NLRP3 polymorphism and dysfunction have been implicated in the pathogenesis of IBD [17, 18]. A seminal study revealed a critical role of the NLRP3 inflammasome in DSS-induced colitis because mice with NLRP3 depletion developed less severe colitis than wild-type mice [19]. In support of the pathogenic roles of the NLRP3 inflammasome in colitis, attenuating the expression of NLRP3 with miR-233 and blocking the NLRP3 inflammasome with the specific MCC950 effectively protect against DSS-induced colitis [20, 21]. Recently, studies have shown that NLRP3 inflammasome activation is positively associated with DSS-induced colitis [22, 23]. However, several studies have shown that the NLRP3 inflammasome may have protective effects against DSS-induced colitis [24, 25]. Other clinical observations revealed a negative association between NLRP3 expression and CD [18]. This discrepancy suggests that the roles of the NLRP3 inflammasome in IBD pathogenesis warrant further investigation.

Recent advances have provided new insight into the mechanisms that regulate NLRP3 inflammasome activation. It is well known that the NLRP3 inflammasome can be triggered by canonical inducers (e.g., extracellular ATP or nigericin) or through the noncanonical pathway downstream of cytosolic LPS-induced caspase-11 activation [14, 26]. Interestingly, potassium ion (K^+) efflux has been identified as a common signal that mediates NLRP3 assembly and is sensed by NEK7 [27]. While nigericin is an ionophore that incorporates into the plasma membrane to form a K^+-permeable channel, ATP-induced K^+ efflux has been shown to be mainly mediated by TWIK2 [28]. In this study, we showed that DSS was unable to directly trigger NLRP3 activation but robustly augmented NLRP3 inflammasome assembly induced by suboptimal ATP or nigericin concentrations. This augmentation of NLRP3 assembly was mainly dependent on intermediate conductance calcium-activated potassium channel protein 4 (KCNN4, also known as KCa3.1). In a mouse model, the severity of DSS-induced colitis was positively associated with the level of inflammasome activation. Pharmacological inhibition or genetic depletion of KCa3.1 greatly mitigated DSS-induced colitis and reduced inflammasome activation, highlighting KCa3.1 as an important mediator of DSS-induced colitis and a therapeutic target for IBD treatment.

MATERIALS AND METHODS

Reagents and antibodies

Dextran sodium sulfate (DSS, #160110, molecular weight: 36–50 kDa) was purchased from MP Biomedicals (Irvine, CA, USA). DSS powder was dissolved in PBS or deionized water to form a 50% solution, sterilized by filtration with a 0.22 μm filter and stored at 4 °C (≤ 1 month). Disuccinimidyl suberate (S1885), propidium iodide (PI) (P4170), ATP (A6419), lipopolysaccharide (LPS) (*Escherichia coli* O111:B4) (L4391), dimethyl sulfoxide (DMSO) (D8418), tetraethylammonium chloride (T2265), ampicillin sodium salt (A9518), N-acetyl-L-cysteine (A7250), Pluronic F-127 (P2443) and Tween-20 (P1379) were purchased from Sigma–Aldrich (St. Louis, MO, USA). Nigericin (tlrl-nig), lipoteichoic acid from *Staphylococcus aureus* (LTA-SA) (tlrl-pslta), poly (dA:dT) (tlrl-patn-1), poly (I:C) (tlrl-picw) and Pam3SCK4 (tlrl-pms) were purchased from InvivoGen (San Diego, CA, USA). Imiquimod (S81181) and probenecid (S24877) were purchased from Yuanye Bio-Technology (Shanghai, China). High-glucose Dulbecco's modified Eagle's medium (DMEM), fetal bovine serum (FBS, #10099141 C), 100× streptomycin and penicillin (#15140122), Opti-MEM (#51985034), Lipofectamine 2000 (#11668030), and Lipofectamine RNAiMAX transfection reagent (#13778075) were obtained from Thermo Fisher/Invitrogen (Carlsbad, CA, USA). Hoechst 33342 (H21492) was purchased from Invitrogen (Carlsbad, CA, USA). FuGENE HD (E2311) was obtained from Promega (Madison, WI, USA). MCC950 (S8930), VX-765 (S2228), TRAM-34 (S1160), BAPTA-AM (S7534), amiodarone (S1979), chlorpromazine (S2456), quinine (S4495), and ML133 (S2825) were purchased from Selleck Chemicals (Houston, TX, USA). Disulfiram (HY-B0240) and NS-6180 (HY-15707) were obtained from MedChemExpress (Princeton, NJ, USA). Metronidazole (B1976), vancomycin hydrochloride (B1223) and neomycin sulfate (B1795) were purchased from APExBIO (Houston, TX, USA).

The anti-NLRP3 antibody (AG-20B-0014) was purchased from Adipogen AG (Liestal, Switzerland). Antibodies against caspase-1 + p10 (ab179515), IL-18 (ab207323), occludin (ab216327), CD3 (ab16669), CD68 (ab125212), and GSDMD (ab209845) were purchased from Abcam (Cambridge, UK). Antibodies against IL-1β (#12242), β-actin (#3700), ASC (#67824), Alexa Fluor 647-conjugated ASC (#23640), α-SMA (#48938), IL-18 (human-specific) (#54943), and GSDMD (human-specific) (#96458), and horseradish peroxidase (HRP)-linked horse anti-mouse IgG (#7076), HRP-linked goat anti-rabbit IgG (#7074), and Alexa Fluor 647-conjugated goat anti-rat IgG (H + L) (#4418 S) were purchased from Cell Signaling Technology (Danvers, MA, USA). Mouse anti-KCa3.1 (sc-365265) and rat anti-Ep-CAM (sc-53532) were purchased from Santa Cruz Biotechnology (Dallas, TX, USA). The rat anti-B220 antibody (#103212) was purchased from BioLegend (San Diego, CA, USA). The rat anti-Ly-6G antibody (#551459) was obtained from BD Biosciences (San Jose, CA, USA). Highly cross-adsorbed CF568-conjugated goat anti-rabbit IgG (H + L) (#20103) and highly cross-adsorbed CF488A-conjugated goat anti-mouse IgG (#20018) were obtained from Biotium (Hayward, CA, USA).

Animals

Wild-type (WT) C57BL/6 J mice (6–8 weeks of age) and heterozygous *Nlrp3*$^{+/-}$ and *Kcnn4*$^{+/-}$ mice on a C57BL/6 J background were purchased from GemPharmatech Co. (Nanjing, China). The *Nlrp3*$^{-/-}$, *Kcnn4*$^{-/-}$ and WT littermates used in this study were produced in-house by breeding heterozygous parents (5–9th generations). Mice with NLRP3 or KCa3.1 deletion had no obvious physiological defects, and their size, body weight and appearance were similar to those of WT littermates. PCR-based genotyping was performed using a Quick Genotyping assay kit for mouse tails (D7283, Beyotime, Shanghai, China) according to the manufacturer's protocol. Specific primers were designed by GemPharmatech (Supplementary Table S1) and synthesized by Sangon Biotech (Shanghai, China). All mice were housed at 24 ± 2 °C on a 12/12-hr light/dark cycle with free access to food and water. Animal housing and experimental procedures were performed with the approval of and in compliance with the guidelines for the care and use of animals approved by the Committee on the Ethics of Animal Experiments of Jinan University.

Cell culture

The mouse J774A.1 cell line was obtained from the Kunming Cell Bank of Type Culture Collection Chinese Academy of Sciences (Kunming, China) and cultured in DMEM supplemented with 10% heat-inactivated FBS, 100 U/mL penicillin and 100 μg/mL streptomycin (complete DMEM). The cells were passaged every 2 days. Bone marrow-derived macrophages (BMDMs) were differentiated as previously described [29]. Briefly, bone

marrow cells from the femurs and tibias of mice were aseptically flushed out with cold PBS. To differentiate the cells into macrophages, pooled bone marrow cells were plated on sterile petri dishes and cultured in complete DMEM containing 20% conditioned medium from L929 cells as a source of M-SCF (MAC medium). Fresh MAC medium was added on the 3rd day of differentiation. Six days later, the differentiated BMDMs were ready for use. All cells were maintained at 37 °C in a 5% CO_2 incubator.

To investigate whether DSS directly triggers NLRP3 inflammasome activation, macrophages were primed with Pam3CSK4 (1 μg/mL) or LPS (0.5 μg/mL) for 4 h, washed with serum-free DMEM and then treated with DSS in Opti-MEM for 16 h. Additionally, cells were primed and washed as described above but were treated with DSS for 1 h and then stimulated with ATP or nigericin. To examine the effects of NLRP3 or caspase-1 inhibitors on the DSS-induced increase in NLRP3 inflammasome activation, LPS-primed cells were treated with DSS plus the indicated concentrations of KCl, disulfiram, MCC950 or VX-765 for 1 h before being stimulated. Pretreatment with other inhibitors was performed for 1 h before DSS treatment.

Cell death assay

Lytic cell death was examined by PI incorporation as previously described [29]. Briefly, cells were seeded in 96-well plates overnight and treated as indicated. Subsequently, an equal volume of serum-free DMEM containing PI (4 μg/mL) and Hoechst 33342 (10 μg/mL) was added to each well and incubated at room temperature for 10 min. The cells were observed by live imaging with a Zeiss Axio Observer D1 microscope (Carl Zeiss, Gottingen, Germany). A series of fluorescence images were captured, and cells that were stained with PI or Hoechst 33342 were counted. The percentage of lytic cell death is represented as the ratio of PI-positive cells (dying cells) to Hoechst 33342-positive cells (all cells).

Immunofluorescence microscopy

For immunofluorescence staining, cells were seeded in glass-bottom cell culture dishes at 1.5×10^5/well overnight. After the appropriate treatments, the cells were fixed with 4% paraformaldehyde for 20 min at room temperature and permeabilized with cold methanol at −20 °C for 10 min. After being washed twice with PBS, the cells were blocked with 5% goat serum in PBS at room temperature for 1 h and then incubated with the appropriate antibodies at 4 °C overnight. On the next day, the cells were washed twice and then incubated with CF488A-conjugated goat anti-mouse IgG or CF568-conjugated goat anti-rabbit IgG at room temperature for 1 h. In some experiments, Alexa Fluor 647-conjugated anti-ASC antibodies were added and incubated following secondary antibody incubation. Cell nuclei were counterstained with Hoechst 33342 (5 μg/mL in PBS) for 15 min. Cell images were captured with a Zeiss Axio Observer D1 inverted fluorescence microscope and analyzed with the built-in ZEN software (Carl Zeiss).

Western blot analysis

For Western blotting, cultured cells and tissues were lysed in 2× sodium dodecyl sulfate–polyacrylamide gel electrophoresis (SDS–PAGE) sample loading buffer containing 200 μM dithiothreitol (DTT), and the cell lysates were sonicated to reduce viscosity. Soluble proteins in the culture supernatants were precipitated with 7.7% trichloroacetic acid plus 0.18% sodium deoxycholate overnight at 4 °C, and the resultant pellets were washed with cold acetone three times and then dissolved in 2× SDS–PAGE sample loading buffer containing DTT. All samples were boiled for 5 min. Equal amounts of protein were separated by SDS–PAGE and electrophoretically transferred to polyvinylidene difluoride (PVDF) membranes. The membranes were blocked with 5% nonfat milk powder in PBS containing 0.1% Tween 20 (PBS-T) for 1 h. After being incubated with the indicated primary antibodies at 4 °C overnight, the membranes were washed with PBS-T and incubated with HRP-conjugated secondary antibodies for 1 h at room temperature. Bands were revealed by a BeyoECL Plus kit (P0018S, Beyotime) and captured on X-ray films. Densitometric analysis of each band was performed by ImageJ, and the intensity of the protein was normalized to β-actin.

ASC oligomer cross-linking

Assembly of the NLRP3 inflammasome was also assessed by ASC oligomer cross-linking [30]. In brief, cells were lysed in ice-cold PBS containing 0.5% Triton X-100 by being sheared 10 times through a 21-gauge needle. The lysates were centrifuged at 10,000 × *g* for 15 min, and the pellets were washed twice with ice-cold PBS and resuspended in 200 μl of PBS containing 2 mM freshly prepared disuccinimidyl suberate (100 mM stock solution in DMSO). ASC oligomers were cross-linked for 30 min at room temperature. After being centrifuged at 10,000 × *g* for 15 min, the resulting pellets were dissolved in 1× SDS–PAGE sample loading buffer containing DTT for Western blot analysis.

RNA interference

Small interfering RNA (siRNA) targeting the murine *Kcnn4* gene (encoding KCa3.1) (5′-CGATCACATTCCTGACCAT-3′) and scramble siRNA (SiN0000001-1-5) were designed and synthesized by RiboBio (Guangzhou, China). Knockdown of *Kcnn4* with 50 nM siRNA in J774A.1 cells was performed by using Lipofectamine RNAiMAX transfection reagent according to the manufacturer's protocol. Cells were collected by scraping 48 h after transfection, counted and then reseeded in a 6-well plate for Western blot analysis or a 96-well plate for PI/Hoechst 33342 staining assays.

Coimmunoprecipitation

The interactions between NEK7, ASC and NLRP3 were analyzed using a coimmunoprecipitation (Co-IP) assay. Briefly, BMDMs were seeded in a 6-well plate overnight and treated routinely to trigger NLRP3 activation. After carefully removing the culture medium, the cells were washed twice with ice-cold PBS and lysed with freshly prepared IP lysis/wash buffer containing PMSF (P0013, Beyotime) in an ice bath for 5 min. Then, the cell lysates were scraped, transferred to cold tubes and sheared 10 times through a 21-gauge needle. After being centrifuged at 13,000 rpm (4 °C) for 10 min, the supernatants were transferred to ice-cold tubes. The protein concentration was measured with a Pierce BCA protein assay kit (#23227, Thermo Scientific), and equal amounts of lysates (140 μg) were subjected to a Co-IP with a Pierce classic IP kit (#26146, Thermo Fisher/Invitrogen) according to the manufacturer's protocol. Briefly, after being precleared with control agarose resin, the lysates were incubated with mouse anti-NLRP3 antibodies or isotype control IgG (0.75 μg antibody/100 μg lysates) at 4 °C overnight. The protein-antibody complexes were captured with Protein A/G agarose and eluted with 2× reducing sample buffer containing DTT in boiling water for 10 min. The abundance of NLRP3, NEK7, and ASC in the elution was analyzed by Western blotting.

Extracellular ion replacement

The replacement of extracellular ions was performed as previously reported [28]. Briefly, LPS-primed macrophages were bathed in homemade low-K^+ (1.25 mM) medium containing DSS (Supplementary Table S2) for 1 h in the presence or absence of MCC950 to determine the effects of DSS on NLRP3 inflammasome activation induced by low extracellular K^+ concentrations. To investigate the roles of K^+, Ca^{2+}, Na^+ and Cl^- in the DSS-induced increase in NLRP3 inflammasome activation, LPS-primed BMDMs were preincubated in homemade medium containing DSS and the indicated concentrations of K^+ (5.4 mM, 15 mM, 30 mM, and 60 mM), Na^+ (145 mM, 135 mM, 120 mM, 90 mM, 72.5 mM, and 0 mM) and Ca^{2+} (2 mM, 1 mM, 0.5 mM, and 0 mM) (Supplementary Table S3) for 1 h, followed by ATP or nigericin stimulation.

Intracellular K^+ measurement

After the appropriate treatments, the culture medium was removed, and the cells were washed with 10 mM phosphate buffer (pH = 7.4) and lysed in deionized water with sonication. The protein concentration of the homogenates was quantified by a BCA protein assay kit. The K^+ concentration was measured by a potassium (K^+) turbidimetric assay kit (E-BC-K279-M, Elabscience, Wuhan, China) according to the manufacturer's protocol, with slight modifications. In brief, 80 μL of homogenate was mixed with an equal volume of commercial protein precipitant, and 50 μL of the supernatant was added to a 96-well plate after being centrifuged at 1100 × *g* for 10 min. Then, 200 μL of the chromogenic agent was added to the wells and mixed fully with the supernatant. After being incubated at room temperature for 5 min, the optical density at 450 nm of each sample was measured with a microplate reader. The resultant K^+ concentration was normalized to the protein concentration in the homogenate lysates. When K^+ channel blockers were used in some experiments, the cells were pretreated with TRAM-34 (5 μM) for 3 h and TEAC (5 mM) and quinine (100 μM) for 0.5 h before LPS priming or were treated with amiodarone (20 μM), chlorpromazine (20 μM), or ML133 (30 μM) for 1 h before DSS treatment and after LPS priming.

Intracellular Ca^{2+} chelation and imaging

The role of intracellular Ca^{2+} in mediating the DSS-induced increase in the NLRP3 inflammasome was examined by blockade with membrane-permeable BAPTA-AM before ATP stimulation. Briefly, after DSS treatment, LPS-primed BMDMs were loaded with BAPTA-AM (1, 2 and 4 μM) for 40 min in Ca^{2+}-free buffer (136 mM NaCl, 5.4 mM KCl, 0.45 mM KH_2PO_4, 1 mM $MgCl_2$, 4.2 mM $NaHCO_3$, 0.34 mM Na_2HPO_3, 5.6 mM glucose, and 10 mM HEPES (pH = 7.4)) supplemented with 0.04% Pluronic F-127 at 37 °C in a 5% CO_2 incubator. Western blotting, CBA, and PI staining were used to evaluate inflammasome activation and pyroptosis. To visualize intracellular Ca^{2+} signaling in response to ATP stimulation, the cells were preloaded with Fluo-4 AM (4 μM) in Ca^{2+}-free buffer containing 0.02% Pluronic F-127 and 1 mM probenecid for 1 h before being stimulated with 1 mM ATP. Whole-cell Ca^{2+} fluorescent images were consecutively recorded during ATP stimulation (every 15 s for at least 10 min) by a Zeiss Axio Observer D1 inverted fluorescence microscope.

DSS-induced colitis

Colitis was induced in mice by 3% DSS, as previously described [25]. Briefly, mice aged 8–10 weeks were subjected to 3% DSS (wt/vol) dissolved in filter-purified drinking water for 5 consecutive days, followed by 2 days of normal drinking water. Control mice were given normal drinking water. Weight loss, rectal bleeding, and diarrhea were monitored and recorded daily up to Day 7. Weight loss was scored as follows: 0, none; 1, 1–5%; 2, 5–10%; 3, 10–20%; and 4, >20%. Stool consistency was scored as follows: 0, well-formed pellets; 1, semisolid and not adhered to the anus; 2, semiformed and adhered to the anus; and 4, liquid stools and adhered to the anus and diarrhea. The bleeding score was assigned as follows: 0, no blood in stool; 1, light and faint; 2, clear and visible; and 4 gross rectal bleeding. The sum of the weight loss, stool consistency and bleeding scores (disease activity index, DAI) was calculated to assess the overall disease severity of each mouse.

To eliminate the influence of the gut microbiota on DSS-induced colitis, *Nlrp3*$^{-/-}$ and sex-matched wild-type littermates (8–10 weeks of age) were cohoused and separated 1 week before DSS administration. To assess the protective effects of TRAM-34 on DSS-induced colitis in mice, female C57BL/6 J mice aged 8–10 weeks were acclimatized for 1 week and then randomly divided into four groups and administered the following treatments: (a) vehicle and DSS-free drinking water (control); (b) TRAM-34 and DSS-free drinking water (TRAM-34); (c) vehicle and 3% DSS-containing drinking water (DSS); and (d) TRAM-34 and 3% DSS-containing drinking water (TRAM-34+DSS). TRAM-34 was freshly prepared in peanut oil at a concentration of 8 mg/mL. TRAM-34 (40 mg/kg body weight) or an equal volume of peanut oil (vehicle) was intraperitoneally injected 1 day before DSS administration and then twice daily until the endpoint.

Histochemical analysis

At the endpoint of the study, the mice were sacrificed, and the colon was isolated. The length of the colon was directly measured with a ruler, and images were captured. The distal colon was then removed and fixed with 10% PBS-buffered formalin, paraffinized and sectioned at a thickness of 4 μm. The sections were stained with hematoxylin and eosin, and the degrees of inflammation and injury were scored as previously described [20].

Immunofluorescence staining

The middle segments of the colon were fixed with 4% paraformaldehyde for 24 h. Frozen sections with a thickness of 8 μm were routinely prepared, and the slides were stored at −20 °C until staining. Immunofluorescence staining was performed as previously described [31], with slight modifications. Before being incubated with primary antibodies, the tissue sections were sequentially equilibrated in PBS at room temperature for 10 min, soaked in sodium citrate-citrate buffer solution (10 mM, pH = 6.0) at 80 °C for 30 min and blocked with PBS containing 5% normal goat serum and 0.1% Triton X-100 for 60 min. The slides were then incubated with the indicated antibodies at 4 °C overnight, followed by incubation with the appropriate mixed fluorescent dye-labeled secondary antibodies for 1 h. After being counterstained with Hoechst 33342 (5 μg/mL in PBS) for 15 min, the tissue sections were covered with antifade mounting medium and coverslips. Fluorescence images were captured by a Zeiss AxioCam MR R3 cooled CCD camera controlled with ZEN software (Carl Zeiss).

Colon organ culture

Colon culture was performed as previously described [31]. Briefly, the colon was longitudinally cut and rinsed with ice-cold PBS three times to completely remove intestinal contents. Then, the colon was cut into 1-cm segments and cultured in 24-well plates with 1 mL of serum-free RPMI-1640 medium containing 1% penicillin–streptomycin for 24 h. Culture supernatants were collected after centrifugation at 5000 rpm for 5 min and immediately stored at −80 °C. To measure caspase-1p10 and the mature forms of IL-1β and IL-18, proteins in the supernatants (equal amounts of each sample) were precipitated with trichloroacetic acid plus sodium deoxycholate at 4 °C overnight, and the resultant pellets were washed with cold acetone three times and then dissolved in 2× SDS–PAGE sample loading buffer containing DTT. After being boiled for 5 min, equal amounts of protein were separated by SDS–PAGE and subjected to Western blot analysis.

Cytokine measurement

Because DSS interferes with the detection of mature IL-1β in culture supernatants by Western blotting, soluble IL-1β in cell culture or colon organ culture supernatants was measured using a cytometric bead array (CBA) mouse IL-1β FlexSet (#560232). Other proinflammatory cytokines, including IL-6 and MCP-1 (CCL-2), were measured using a CBA mouse inflammation kit (#552364) according to the manufacturer's instructions (BD Biosciences, San Jose, CA, USA). Data were acquired using an Attune NxT Acoustic Focusing Cytometer (Life Technologies, Thermo Fisher Scientific) and analyzed with FlowJo V10 software (BD Biosciences). The measured concentrations of each cytokine in colon organ culture supernatants were normalized to the total protein concentration (pg/mg protein).

Statistical analysis

In vitro experiments were performed at least three times independently. The data are expressed as the mean ± standard deviation (SD) and were analyzed using GraphPad Prism 5.0 (GraphPad Software Inc., San Diego, CA, USA). The statistical significance of multiple comparisons was analyzed using one-way analysis of variance (ANOVA) followed by the Bonferroni *post hoc* test, and unpaired Student's *t* test was used for two-group comparisons. $P < 0.05$ were considered statistically significant.

RESULTS

Genetic depletion of NLRP3 decreases DSS-induced colitis and reduces inflammasome activation in the colon

In recent decades, many studies on genetically modified mice have been performed, but the role of the NLRP3 inflammasome in DSS-induced colitis remains controversial, as both protection [19] and deterioration [24, 25] have been observed in NLRP3-deficient mice. These differences may be attributed to multiple variables, including the DSS dose, experimental environment, and genetic background [32]. To eliminate the potential interference of the experimental environment and genetic background, *Nlrp3*$^{-/-}$ mice and their wild-type (WT) littermates (*Nlrp3*$^{+/+}$) were bred in house (Fig. 1A). The effect of the gut microbiota on DSS-induced colitis was minimized as *Nlrp3*$^{-/-}$ mice and their sex-matched *Nlrp3*$^{+/+}$ littermates were cohoused and separated 1 week before DSS administration. To induce acute colitis, the mice were given free access to drinking water containing 3% DSS for 5 consecutive days followed by normal drinking water for 2 additional days. The body weights of WT and *Nlrp3*$^{-/-}$ mice decreased over time with DSS intake, but weight loss in WT mice was more severe than that in *Nlrp3*$^{-/-}$ mice (Fig. 1B). Consistently, the accumulated disease activity index (DAI) of WT mice was higher than that of *Nlrp3*$^{-/-}$ mice at the later time points of DSS exposure (Fig. 1C). In addition, the colons of unexposed WT and *Nlrp3*$^{-/-}$ mice had comparable lengths; DSS-exposed mice had shortened, congested and edematous colons, but these symptoms were ameliorated in *Nlrp3*$^{-/-}$ mice compared with their WT littermates (Fig. 1D, E). These macroscopic observations indicate that NLRP3 depletion protects against DSS-induced colitis in mice.

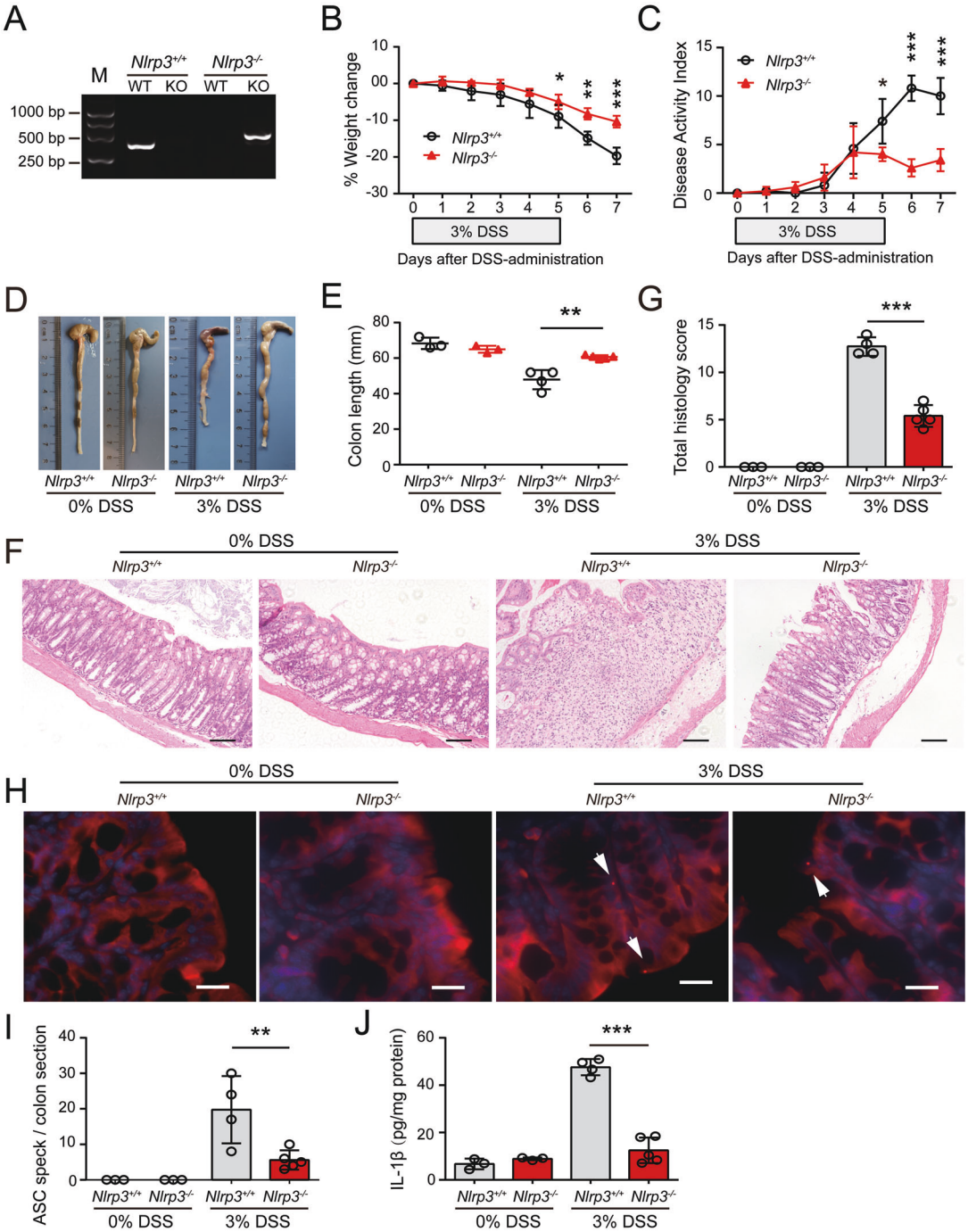

Fig. 1 NLRP3 deficiency attenuates DSS-induced colitis and inflammasome activation in mice. *Nlrp3*$^{-/-}$ and *Nlrp3*$^{+/+}$ littermates were treated with 3% DSS dissolved in drinking water for 5 days and DSS-free drinking water for another two days. **A** Wild-type and *Nlrp3* knockout mice were identified by PCR with specific primers. Representative electrophoretic analysis of PCR products from *Nlrp3*$^{+/+}$ (446 bp) and *Nlrp3*$^{-/-}$ (559 bp) mice is shown. **B** NLRP3 depletion protected mice from DSS-induced weight loss. Weight loss during DSS treatment is expressed as the percent change from Day 0. **C** NLRP3 depletion protected mice from DSS-induced increases in DAI scores. Weight loss, diarrhea and rectal bleeding were recorded and scored daily; the DAI score was the sum of these scores. **D**, **E** NLRP3 depletion protected the colon from DSS-induced shortening. Representative photographs of the colon in each group are shown (**D**), and the length of the colon was compared among groups (**E**). **F**, **G** NLRP3 depletion protected the colon against DSS-induced injuries and immune cell infiltration. Representative images of colonic sections (H&E. staining) are shown (**F**). Scale bars, 100 μm. The histology score of each colon section was quantified and compared among groups (**G**). **H**, **I** NLRP3 depletion inhibited ASC speck formation in the DSS-exposed colon. Frozen sections of the colon were obtained and incubated with antibodies against ASC, and nuclei were counterstained with Hoechst 33342. Representative immunofluorescence images of colonic ASC are shown, and white arrows indicate ASC specks (**H**). Scale bars, 20 μm. The number of ASC specks in each colonic section was quantified (**I**). **J** NLRP3 depletion decreased the release of IL-1β from the DSS-exposed colon. The proximal colon (1–2 cm) was opened longitudinally and incubated in serum-free RPMI-1640 medium at 37 °C (5% CO_2) for 24 h. The concentration of IL-1β in the supernatants was measured by a cytometric bead array and normalized to the total protein concentration (pg/mg protein). The data are expressed as the mean ± SD, and statistical analyses were performed using Student's t test. *$p < 0.05$, **$p < 0.01$, ***$p < 0.001$

Next, we microscopically examined tissue injury and inflammation in the colons of mice by hematoxylin and eosin (H&E.) staining and immunofluorescence analysis. In the absence of DSS administration, *Nlrp3*$^{-/-}$ mice and their WT littermates had normal crypts and epithelial cells (Ep-CAM^{+}) and high expression of occludin in the colon (Fig. 1F, Fig. S1A). After DSS treatment, however, multiple ulcerative lesions were observed in the colons of WT mice, and the crypts and epithelial cells were almost completely lost, the expression of occludin was decreased, and inflammatory cells, including macrophages (CD68^{+}) and neutrophils (Ly-6G^{+}), were heavily infiltrated, while the numbers of B (B220^{+}) and T cells (CD3^{+}) were only slightly increased in ulcerative lesions (Fig. 1F, Fig. S1A–C). Notably, NLRP3 depletion markedly reduced the severity of DSS-induced tissue injury (Fig. 1F, G), increased the expression of occludin, and reduced the infiltration of inflammatory cells in the colon (Fig. S1A–C).

We also examined ASC speck formation as a surrogate marker of inflammasome assembly in the colon by immunofluorescence microscopy. An ASC speck was defined as a perinuclear spot with strong ASC fluorescence. ASC specks were detected in the colons of WT mice after DSS exposure, but none were observed in the absence of DSS treatment. Moreover, NLRP3 depletion significantly decreased the formation of ASC specks in the DSS-exposed colon (Fig. 1H, I), which indicated reduced inflammasome assembly. Consistently, lower levels of IL-1β were detected in the medium of colon organ cultures from NLRP3-deficient mice compared with WT littermates (Fig. 1J). Furthermore, fluorescence microscopy showed that both macrophages (CD68^{+}) and intestinal epithelial cells (IECs) (Ep-CAM^{+}) formed ASC specks in response to DSS exposure (Fig. S2A). Notably, although NLRP3 depletion almost completely abrogated ASC specks in macrophages, it significantly decreased but did not fully block the formation of ASC specks in IECs (Fig. S2B, C), suggesting that ASC speck formation in IECs in response to DSS treatment was mediated partly by NLRP3 and other inflammasome sensors. Supporting its role in IECs, NLRP3 protein expression was markedly upregulated in IECs in response to DSS exposure (Fig. S2D, E), which was presumably induced by tissue injury and/or gut microbes crossing the disrupted mucosal layers. Thus, in the DSS-exposed colon, ASC speck formation in macrophages was largely dependent on NLRP3, but ASC speck formation in IECs as mediated by both NLRP3 and other inflammasome sensors.

Previous studies showed that NLRP3 depletion may affect the intestinal microflora, thus attenuating DSS-induced colitis [33], and we examined whether the gut microbiota mitigated the severity of colitis in our experimental setting. We performed fecal microbiota transfer (FMT) experiments from *Nlrp3*$^{-/-}$ mice or their *Nlrp3*$^{+/+}$ littermates to WT mice. After depleting the gut microbiota with an antibiotic cocktail (ABX), WT mice were recolonized with the fecal microbiota from *Nlrp3*$^{-/-}$ or *Nlrp3*$^{+/+}$ littermates and then subjected to DSS treatment (Fig. S3A). Two weeks of treatment with ABX almost completely depleted the gut microbiota, as revealed by the PCR results (Fig. S3B), and ABX treatment slightly decreased the sensitivity of mice to DSS-induced colitis at the endpoint of the experiment (Fig. S3C–H, ABX-treated *versus* untreated). Notably, ABX-treated mice that received fecal microbiota from *Nlrp3*$^{-/-}$ mice (KO → WT) exhibited similar sensitivity to DSS-induced colitis as those that received fecal microbiota from *Nlrp3*$^{+/+}$ littermates (WT → WT) (Fig. S3C–H), suggesting that the gut microbiota had a minor contribution to mitigating DSS-induced colitis in NLRP3-depleted mice under this experimental setting.

Taken together, these results indicate that NLRP3 inflammasome activation plays a critical role in mediating DSS-induced colitis in mice.

DSS does not directly trigger but does potentiate NLRP3 inflammasome assembly induced by canonical stimulants

Having shown that NLRP3 depletion ameliorated DSS-induced colitis and reduced inflammasome activation in vivo, we next examined the effects of DSS on NLRP3 inflammasome and pyroptosis activation in macrophages in vitro, as previous studies have shown that DSS could directly activate the NLRP3 inflammasome in LPS-primed macrophages [19]. Bone marrow-derived macrophages (BMDMs) were primed with Pam3CSK4 (TLR2 activator) or LPS (TLR4 activator) for 4 h and then treated with DSS for 16 h after Pam3CSK4 or LPS was washed out. Unexpectedly, the autoprocessing of pro-caspase-1, the release of the caspase-1p10 fragment, the maturation and release of IL-18 into culture supernatants, and the conversion of full-length GSDMD to pyroptotic GSDMD-NT in LPS- and Pam3CSK4-primed BMDMs were not detectable by Western blot analysis (Fig. S4A). Consistently, neither apoptotic morphology nor lytic cell death (revealed by propidium iodide (PI) incorporation) was observed in cells treated with DSS (Fig. S4B).

Thus, these results demonstrated that DSS alone was unable to trigger NLRP3 inflammasome activation in LPS- or Pam3CSK4-primed macrophages. We therefore examined whether DSS could affect canonical NLRP3 inflammasome activation. After LPS priming and the washing steps, the cells were pretreated with vehicle or DSS and exposed to suboptimal doses of ATP (2 mM) or nigericin (1 μM). Such low doses of ATP or nigericin only weakly activated the NLRP3 inflammasome, as indicated by the low levels of released caspase-1p10, IL-1β, IL-18, and cleaved GSDMD-NT (Fig. 2A–D, Fig. S5A–D). However, DSS markedly increased the levels of these proteins in a dose-dependent manner, indicating augmented activation of the NLRP3 inflammasome. Of note, DSS treatment overtly decreased the mobility (i.e., apparent molecular weight) of cellular proteins such as pro-IL-1β, pro-caspase-1, GSDMD-NT and β-actin, as shown by in Western blotting (Fig. 2A, B and other data in following figures), which might be caused by the binding of DSS to these proteins when DSS enters the cells following the disruption of the plasma membrane, possibly leading to increased molecular sizes and/or abnormal SDS incorporation into the proteins, given that DSS is a polymer with a high density of negative charges [11]. Furthermore, lytic cell death was greatly enhanced by DSS pretreatment in both BMDMs (Fig. 2E–G) and J774A.1 cells (Fig. S5E), suggesting markedly increased pyroptosis but not secondary necrosis or necroptosis because neither GSDME cleavage nor MLKL phosphorylation was detectable (Fig. S6). Consistent with the increase in inflammasome activation, ASC speck formation and ASC oligomerization were also markedly increased in the presence of DSS compared to the effect of ATP or nigericin alone (Fig. S7A–E). Interestingly, DSS also significantly increased ATP- and nigericin-induced inflammasome activation and pyroptosis in human THP-1-derived macrophages (Fig. S5F–H). In macrophages, there are other inflammasome sensors, including NLRC4, AIM2, and NLRP6 [13]., which can be activated by flagellin, poly(dA:dT), and LTA-SA, respectively [34–36]. We thus asked then examined whether DSS affected the activation of these inflammasomes in response to treatment with their cognate inducers. The results showed that NLRP6, NLRC4 and AIM2 inflammasomes were markedly activated by transfection with LTA-SA, flagellin, and poly(dA:dT), respectively, as revealed by the cleavage of caspase-1 and GSDMD, as well as the release of IL-18 and/or IL-1β, all of which were unaffected or slightly suppressed by DSS Fig. S8A–C). Furthermore, pyroptotic cell death following the activation of these inflammasomes was barely affected by DSS treatment (Fig. S8D). Taken together, these results suggest that DSS specifically and preferably potentiates ATP- or nigericin-induced NLRP3 inflammasome activation in macrophages to a certain extent.

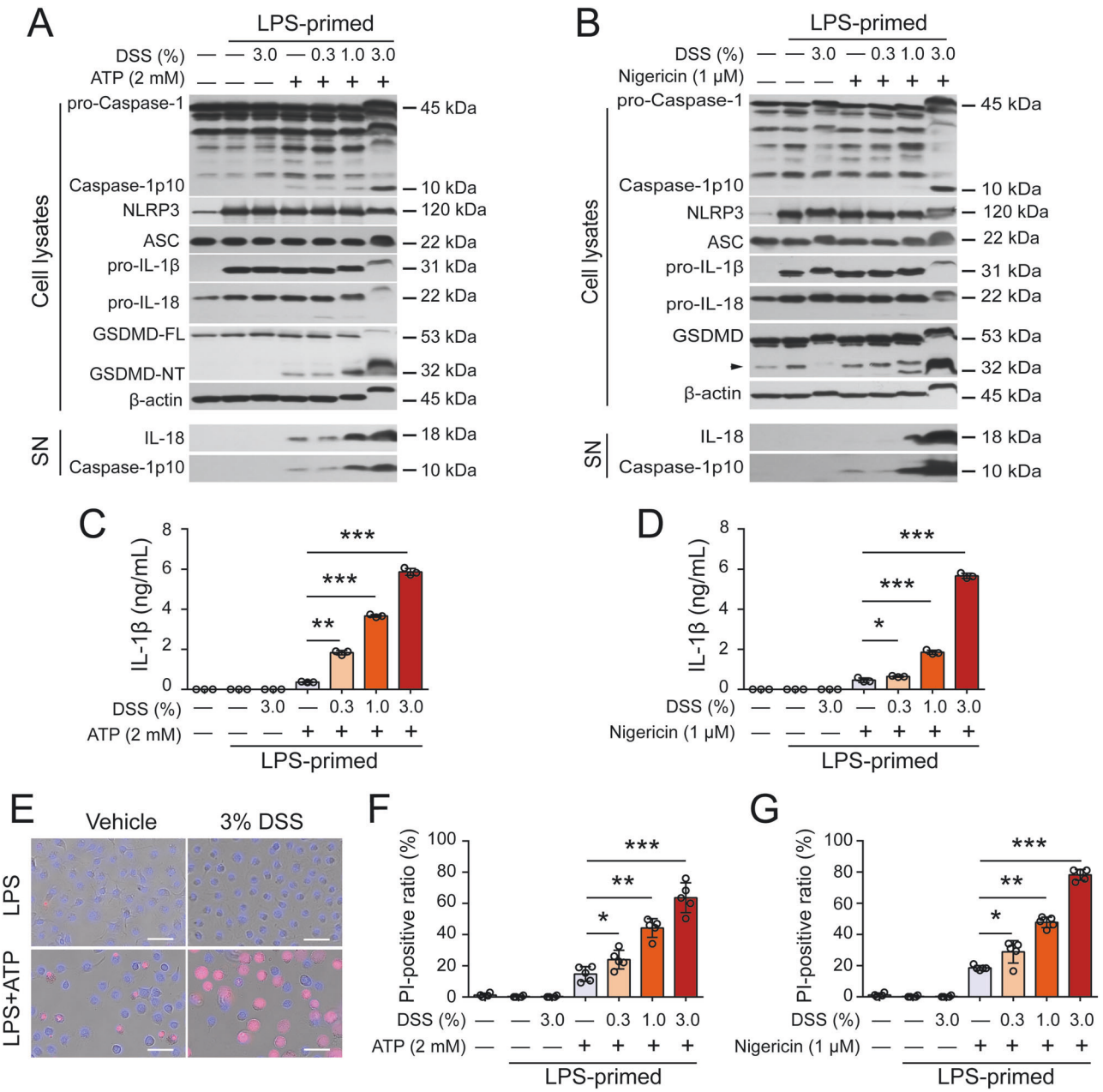

Fig. 2 DSS augments ATP- or nigericin-induced NLRP3 inflammasome activation and pyroptosis in macrophages. Bone marrow-derived macrophages (BMDMs) were differentiated from the bone marrow cells of C57BL/6J mice. After being primed with LPS (0.5 μg/mL) for 4 h, the cells were treated with DSS for 1 h followed by ATP (2 mM, 30 min) and nigericin (1 μM, 1 h) stimulation. The indicated proteins in precipitated proteins from culture supernatants (SN) and cell lysates were examined by Western blot analysis. β-Actin was used as a loading control for cell lysates. **A**, **B** DSS dose-dependently enhanced inflammasome activation triggered by ATP (**A**) or nigericin (**B**). The arrowhead denotes nonspecific bands. **C**, **D** DSS promoted the release of IL-1β from macrophages stimulated with ATP (**C**) or nigericin (**D**). The levels of IL-1β in the supernatants were measured with a cytometric bead assay. **E** DSS changed the morphological characteristics of dying cells. Cell death was determined by PI/Hoechst 33342 staining. One set of representative images from three independent experiments is shown. Scale bars, 50 μm. **F**, **G** DSS dose-dependently increased the percentage of lytic cell death triggered by ATP (**F**) or nigericin (**G**). The ratios of PI-positive cells in 5 randomly chosen fields were quantified. The data are expressed as the mean ± SD. *$p < 0.05$, **$p < 0.01$, ***$p < 0.001$

To further validate the role of the NLRP3 pathway in the DSS-induced increase in inflammasome activation, specific inhibitors and NLRP3 depletion were used in the following experiments. First, the specific NLRP3 inhibitor MCC950 [37] not only abrogated the release of caspase-1p10, IL-1β, and IL-18 into the culture supernatant but also blocked the cleavage of GSDMD and PI uptake in BMDMs treated with DSS and ATP (Fig. 3A–C). Similar results were observed in response to nigericin, and inflammasome assembly and activation were blocked by MCC950 (Fig. S9A–C). The caspase-1-specific inhibitor VX-765 also dose-dependently abrogated these increases in inflammasome activation and pyroptosis (Fig. 3A–C, Fig. S9A, B). In addition, the GSDMD-NT inhibitor disulfiram decreased IL-1β release and PI uptake in ATP- or nigericin-treated cells in the presence of DSS (Fig. S9D–G). Furthermore, genetic depletion of NLRP3 not only fully abrogated the release of caspase-1p10, IL-1β, and IL-18 but also blocked the cleavage of GSDMD and PI uptake (indicating pyroptosis) (Fig. 3D–F, Fig. S9H, I). Overall, these results indicate that DSS

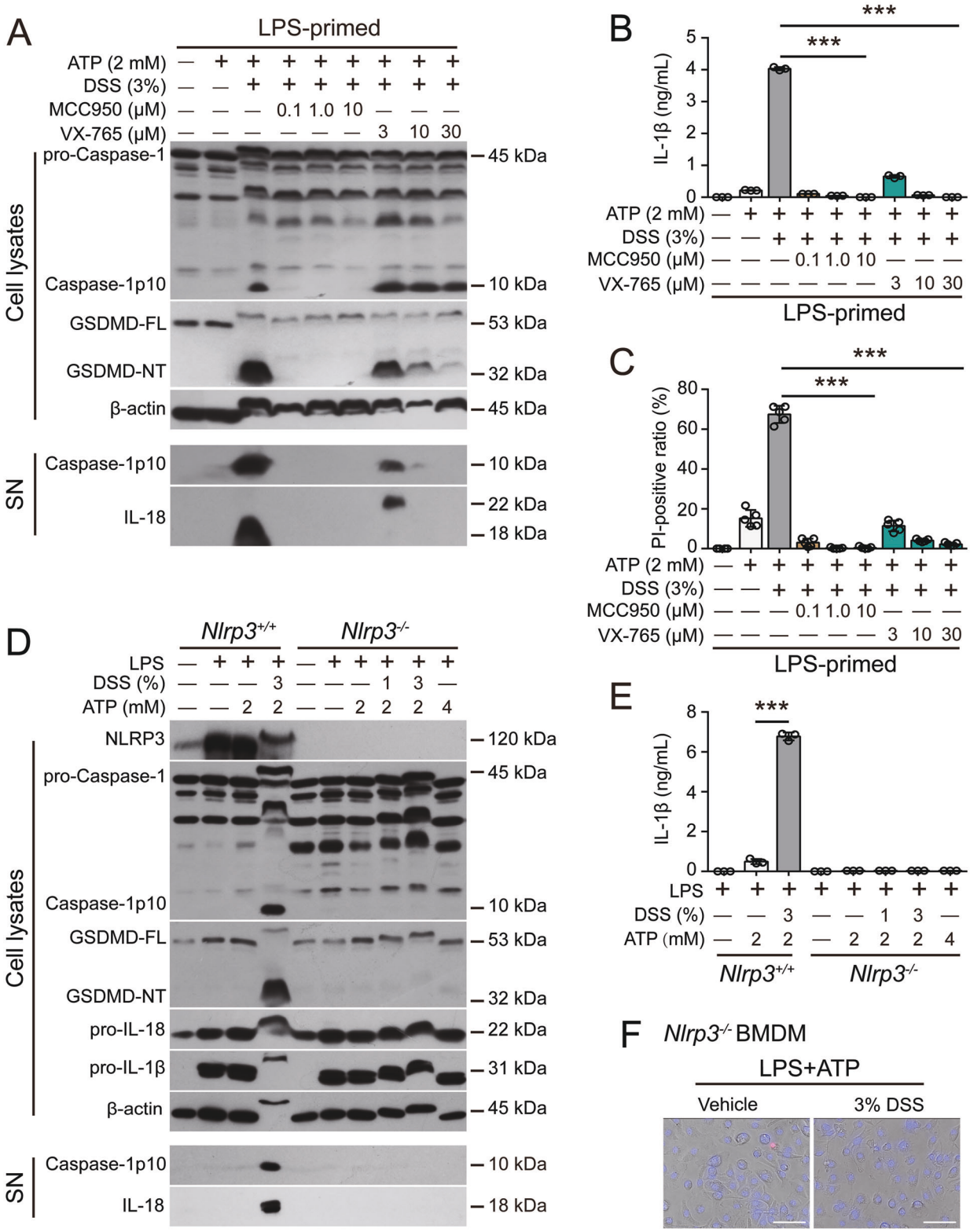

Fig. 3 NLRP3 inhibition and depletion abrogate the DSS-induced increase in ATP-induced inflammasome activation. BMDMs derived from *Nlrp3*$^{-/-}$ mice and their *Nlrp3*$^{+/+}$ littermates were differentiated and treated as described in Fig. 1. Cells were pretreated with a specific inhibitor and DSS and then stimulated with ATP for 30 min. Western blotting was used to examine the indicated proteins in cell lysates and precipitated proteins from culture supernatants (SN). IL-1β levels in culture supernatants were measured by CBA. Lytic cell death was determined by PI/Hoechst 33342 staining, and the ratios of PI-positive cells in 5 randomly chosen fields were quantified. In addition, merged images showing PI and Hoechst 33342 fluorescence and bright-field images are shown. Scale bars, 50 μm. **A–C** MCC950 or VX-765 treatment blocked DSS-mediated enhancement of ATP-induced inflammasome activation (**A**), IL-1β secretion (**B**) and lytic cell death (**C**) in WT cells. **D–F** NLRP3 depletion blocked ATP-induced inflammasome activation (**D**), IL-1β secretion (**E**) and lytic cell death (**F**) in the presence of DSS. The data are expressed as the mean ± SD. ***$p < 0.001$

does not trigger inflammasome assembly but augments ATP- or nigericin-induced inflammasome activation and pyroptosis via the NLRP3/caspase-1/GSDMD pathway.

DSS-induced potentiation of NLRP3 inflammasome assembly depends on potassium ion efflux

Next, we investigated the possible mechanisms underlying the DSS-induced increase in canonical NLRP3 inflammasome activation. Because K^+ efflux is generally believed to be a common trigger of NLRP3 inflammasome assembly [14], we examined the role of K^+ in this process. Interestingly, the DSS-induced increases in ATP- or nigericin-induced NLRP3 inflammasome activation and pyroptosis were dose-dependently blocked by solutions containing high extracellular K^+ but not Na^+ or Ca^{2+}, even though low extracellular Ca^{2+} slightly decreased DSS- and ATP-induced lytic cell death (Figs. S10A–E, S11A–F). In addition, DSS dose-dependently enhanced NLRP3 activation and pyroptosis induced by low K^+ medium, and these effects were effectively blocked by MCC950 (Fig. S12A–G). However, inflammasome activation (Fig. S13A) and pyroptosis (Fig. S13B) induced by imiquimod, a K^+ efflux-independent NLRP3 activator [38], were minimally affected by DSS pretreatment, suggesting that DSS had no effect on K^+ efflux-independent activation of the NLRP3 inflammasome. We thus concluded that DSS influenced K^+ efflux. As expected, DSS pretreatment not only decreased the intracellular K^+ concentration in response to ATP or nigericin stimulation in *Nlrp3*$^{-/-}$ BMDMs but also further decreased K^+ levels induced by low extracellular K^+ concentrations, whereas DSS alone had no effect on K^+ efflux (Fig. 4A–C), indicating that DSS accelerated rather than triggered K^+ efflux. Consistent with this finding, the K^+ efflux-induced interaction between NEK7 and NLRP3 was intensified in the presence of DSS (Fig. 4D, E). Taken together, these results indicate that DSS potentiates ATP- or nigericin-induced NLRP3 activation by enhancing K^+ efflux, which is triggered by canonical stimulators.

Intermediate conductance calcium-activated potassium channel 4 (KCa3.1) is critical for DSS-mediated potentiation of NLRP3 inflammasome assembly and pyroptosis

Given the results showing that K^+ efflux played a critical role in the enhancement of NLRP3 inflammasome activation by DSS and that DSS could promote K^+ efflux induced by ATP, nigericin, and low levels of extracellular K^+, we hypothesized that certain K^+ channel(s) are involved in this process. In addition to nigericin-mediated K^+/H^+ antiport and ATP-mediated opening of the nonselective cation channel P2X7R, K^+ can also flow out through selective K^+ channels, including two-pore domain K^+ channels (e.g., TWIK2), calcium-activated K^+ channels (e.g., KCa3.1), voltage-gated K^+ channels (e.g., Kv3.1), ATP-sensitive K^+ channels and inward rectifier K^+ channels (e.g., Kir2.1), under physiological and/or stressed conditions [28, 39, 40]. We first evaluated the effects of well-known K^+ channels that are involved in NLRP3 inflammasome activation, including P2X7R, TWIK2 and pannexin-1, on the DSS-induced increase in NLRP3 inflammasome activation. Although blocking P2X7R with A-804598 effectively inhibited ATP-induced inflammasome activation and pyroptosis even in the presence of DSS, it did not alleviate the effect of DSS on enhancing nigericin-induced inflammasome activation and pyroptosis (Fig. S14A–C). Consistent with previous studies [28], pretreatment with quinine (a TWIK2 inhibitor) significantly inhibited ATP-induced NLRP3 inflammasome activation but unexpectedly failed to reverse the enhancement of inflammasome activation in the presence of ATP and DSS (Fig. S15A, B). In addition, blocking the pannexin-1 K^+ channel with trovafloxacin did not attenuate the DSS-induced increases in NLRP3 inflammasome activation and pyroptosis in BMDMs (Fig. S15C–E).

Subsequently, we screened several typical K^+ channel inhibitors, including TRAM-34 (KCa3.1 inhibitor), tetraethylammonium chloride (voltage-gated K^+ channel inhibitor), chlorpromazine (inhibitor of nonselective inward rectifier K^+ and time-independent outward rectifier ion channel), amiodarone (Na^+/K^+-ATPase inhibitor), and ML133 (Kir2.1 inhibitor), by Western blotting and PI incorporation (as a surrogate of pyroptosis) assays. Intriguingly, TRAM-34 not only effectively inhibited the DSS-induced increase in NLRP3 inflammasome activation and subsequent pyroptosis in the presence of ATP (Fig. 5A, B) but also suppressed these processes in the presence of nigericin (Fig. S16A–C), whereas the other inhibitors showed no significant effects (Fig. 5A, B). The dose-dependent inhibitory effects of TRAM-34 were further reinforced by its ability to reverse the release of caspase-1p10, IL-18, and IL-1β, as well as ASC oligomerization and ASC speck formation (Fig. 5C–E). Consistent with this finding, the KCa3.1 inhibitor NS-6180 exerted similar inhibitory effects (Fig. S16D, E). In addition, the robust activation of the NLRP3 inflammasome in BMDMs triggered by high-dose ATP (5 mM) or nigericin (20 μM), in the absence of DSS was partly inhibited by TRAM-34 (Fig. S17A–C), suggesting that KCa3.1 might play a role in this process, but this finding needs further clarification. Importantly, blocking KCa3.1 with TRAM-34 significantly reversed the DSS-induced increase in K^+ efflux induced by ATP or nigericin (Fig. 5F, G), further verifying the critical role of the K^+ channel in this process. On the other hand, TRAM-34 had no effect on ROS levels in BMDMs treated with DSS plus ATP (Fig. S18A–C), suggesting a minimal role of ROS. Indeed, blocking intracellular ROS with NAC failed to affect the DSS-induced increase in NLRP3 inflammasome activation (Fig. S18D, E).

Considering that KCa3.1 is a Ca^{2+}-activated K^+ channel [40], we examined whether intracellular Ca^{2+} signaling was required for the KCa3.1 channel to mediate the DSS-induced increase in NLRP3 inflammasome activation and K^+ efflux. The results showed that the DSS-induced enhancement of NLRP3 inflammasome activation was significantly attenuated in cells that were preloaded with the membrane-permeable Ca^{2+}-chelating reagent BAPTA-AM prior to ATP stimulation (Fig. 5H–K). BAPTA-AM treatment also diminished the enhanced efflux of K^+ induced by ATP plus DSS (Fig. 5L), indicating that the DSS-induced increase in the KCa3.1 channel activity was dependent on Ca^{2+} signaling. However, the calcium fluorescent indicator Fluo-4 showed that ATP-induced intracellular Ca^{2+} signaling was largely unaffected by DSS cotreatment (Fig. S19), suggesting that DSS did not affect Ca^{2+} release from intracellular pools or influx from the extracellular compartment and that DSS might act on the KCa3.1 channel to enhance its function when it had been triggered by Ca^{2+} signaling, but this conclusion needs further investigation.

To further validate the role of KCa3.1, we knocked down *Kcnn4* gene (encoding KCa3.1) expression by small-interfering RNAs or knocked out the *Kcnn4* gene in mice by using the CRISPR/cas9 system. Knockdown of *Kcnn4* in J774A.1 macrophages significantly suppressed NLRP3 inflammasome activation and pyroptosis in response to DSS plus ATP (Fig. 6A–D). Furthermore, BMDMs from *Kcnn4*$^{-/-}$ mice exhibited reduced NLRP3 inflammasome activation, pyroptosis and K^+ efflux compared with those from their WT littermates (Fig. 6E–J). These results indicate that the K^+ channel KCa3.1 has a critical role in mediating the DSS-induced increase in NLRP3 inflammasome activation and pyroptosis.

Blockade of KCa3.1 alleviates DSS-induced colitis and decreases inflammasome activation in the colon

Because the results show that KCa3.1 plays a critical role in mediating the DSS-induced increase in NLRP3 inflammasome activation in vitro, we next examined whether pharmacological blockade of KCa3.1 could ameliorate DSS-induced intestinal injury, inflammasome activation and colitis in mice. TRAM-34 was intraperitoneally administered twice daily starting one day before DSS treatment and consecutively until the day before sacrifice. In the absence of DSS exposure, the body weights of mice

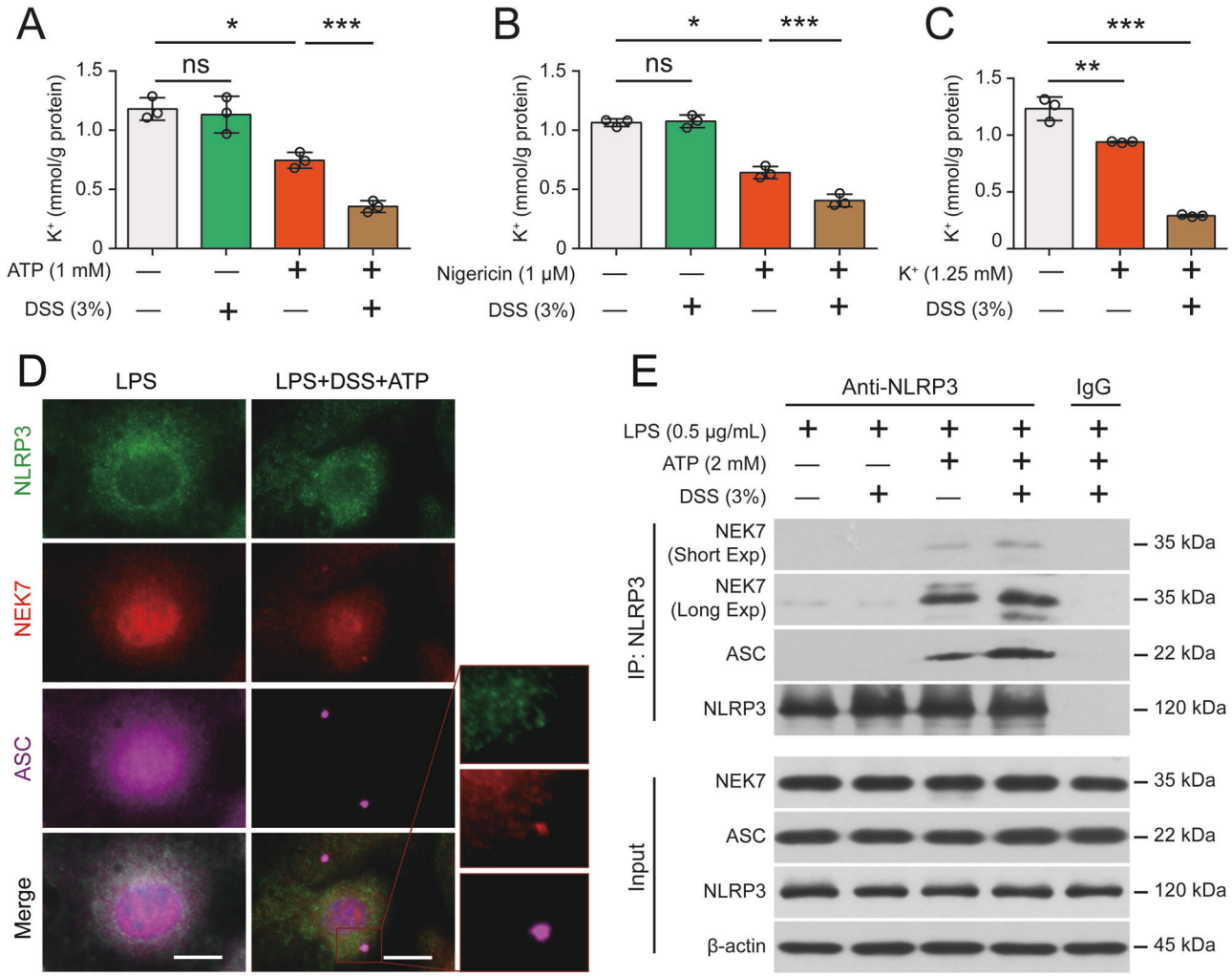

Fig. 4 DSS augments K^+ efflux and the subsequent NEK7-NLRP3 interaction during NLRP3 activation. **A–C** DSS enhanced the efflux of K^+ from cells stimulated with ATP (**A**), nigericin (**B**) and low extracellular K^+ concentrations (**C**). BMDMs were differentiated from the bone marrow cells of *Nlrp3*$^{-/-}$ mice. After the cells were primed with LPS for 4 h, the LPS was removed, and the cells were treated with DSS and then stimulated with 1 mM ATP for 10 min (**A**), 1 μM nigericin for 10 min (**B**) or low extracellular K^+ (1.25 mM) medium for 30 min (**C**). **D**, **E** The ATP-induced NLRP3-NEK7 interaction was enhanced by DSS pretreatment. Immunofluorescence staining revealed the colocalization of NEK7 and ASC specks after the indicated treatments (**D**). Scale bars, 10 μm. A Co-IP assay was performed to assess the interaction of NEK7 and NLRP3 after the indicated treatments (**E**). The data are expressed as the mean ± SD, and statistical analyses were performed using ANOVA followed by Bonferroni *post hoc* test. ns, not significant. *$p < 0.05$, ***$p < 0.001$

administered vehicle (peanut oil) or TRAM-34 were slightly increased. In response to DSS treatment, the body weights of vehicle-treated mice were decreased from Day 4 to the endpoint (Day 7), whereas TRAM-34 administration effectively prevented the DSS-induced loss of body weight (Fig. 7A). In addition, peanut oil or TRAM-34 alone (i.e., without DSS) did not induce changes in stool consistency or hematochezia in mice and thus did not increase their DAI scores; in contrast, the DAI scores were increased from Day 3 onward after DSS exposure and were markedly decreased by TRAM-34 administration (Fig. 7B). DSS-induced diarrhea and hematochezia were mitigated by TRAM-34 (data not shown). Consistent with these results, TRAM-34 treatment also effectively prevented the shortening of the colon in DSS-exposed mice but did not change the colon length in control mice exposed to drinking water (Fig. 7C, D).

After the macroscopic examination, the colon was subjected to histochemical staining and immunofluorescence microscopy. As shown in Fig. 7E, no obvious injury or inflammatory cell infiltration was observed in the colons of vehicle- and TRAM-34-treated mice in the absence of DSS treatment. TRAM-34 administration greatly reduced DSS-induced intestinal injury, the loss of the epithelium and crypts, and the infiltration of inflammatory cells in colons compared with the vehicle controls (Fig. 7E, F). In particular, the infiltration of $CD68^+$ macrophages, the loss of $Ep\text{-}CAM^+$ epithelial cells, the downregulation of the tight junction protein occludin and the overproduction of MCP-1 (CCL2) and IL-6 were markedly mitigated by TRAM-34 compared with the vehicle (Fig. S20A–E).

We next investigated whether inflammasome activation in the mouse colon was associated with DSS-induced colitis. As shown in Fig. 7G, vehicle and TRAM-34 administration did not cause the formation of ASC specks in the colon in the absence of DSS treatment. However, DSS treatment obviously induced the formation of ASC specks in the colon, and this effect was markedly reduced by TRAM-34 administration (Fig. 7G, H). Consistently, TRAM-34 treatment markedly decreased the amount of caspase-1p10, IL-1β and IL-18 released from the colon in mice treated with DSS (Fig. 7I, J). These results indicate that DSS-induced colitis involves KCa3.1-regulated inflammasome activation in the colon.

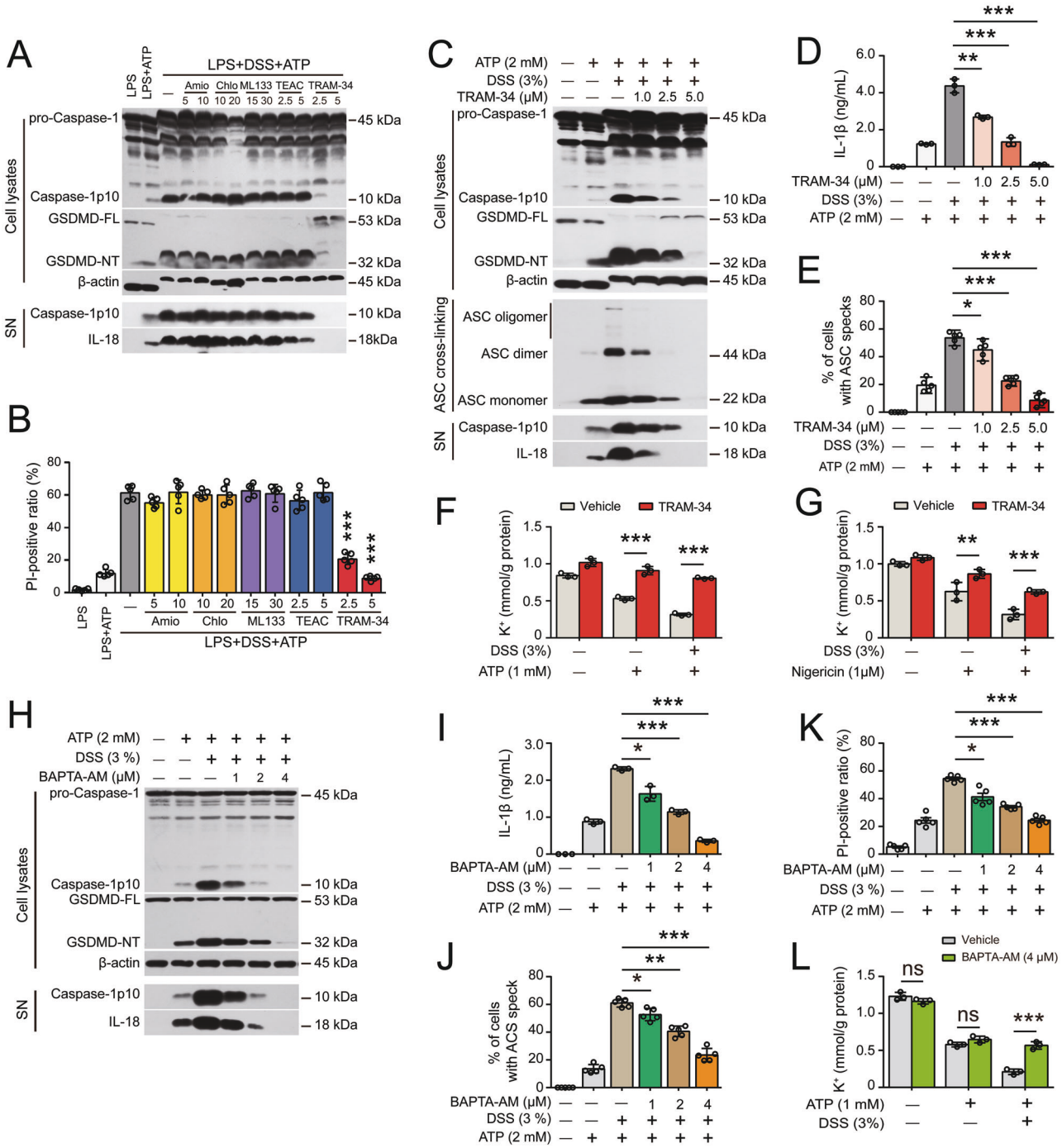

Fig. 5 Blocking the KCa3.1 channel attenuates the DSS-induced increase in NLRP3 inflammasome activation by suppressing K^+ efflux. After being primed with LPS for 4 h, BMDMs were treated with DSS for 1 h and then stimulated with ATP (30 min). K^+ channel inhibitors were added and incubated as follows: TRAM-34 and tetraethylammonium chloride (TEAC) were added before LPS priming for 1 h; and amiodarone (Amio), chlorpromazine (Chlo) and ML133 were added after LPS priming but before DSS for 1 h. The indicated proteins in cell lysates and culture supernatants (SN) were assayed by Western blotting. ASC oligomerization was determined by using ASC crosslinking and immunofluorescence staining. Lytic cell death was determined using PI/Hoechst 33342 staining, and the ratios of PI-positive cells in 5 randomly chosen fields were quantified. IL-1β levels in supernatants were measured with a CBA. The K^+ concentration in the cell lysates was measured by a potassium (K^+) turbidimetric assay and normalized to the protein concentration in the homogenate (mM/g protein). **A**, **B** The effects of several selected K^+ channel inhibitors on DSS-mediated promotion of ATP-induced inflammasome activation (**A**) and lytic cell death (**B**). **C–E** TRAM-34 dose-dependently attenuated the DSS-induced increase in ATP-induced inflammasome activation (**C**), IL-1β secretion (**D**) and ASC speck formation (**E**). After sequential treatment with TRAM-34, LPS and DSS, BMDMs were stimulated with ATP (30 min) to activate the NLRP3 inflammasome. **F**, **G** TRAM-34 treatment reversed the DSS-induced enhancement of ATP (**F**)- and nigericin (**G**)-induced K^+ efflux. K^+ efflux was induced by ATP (1 mM, 10 min) and nigericin (1 μM, 10 min). **H–L** Blocking intracellular Ca^{2+} signaling with BAPTA-AM abrogated the DSS-induced increases in ATP-induced inflammasome activation (**H**), IL-1β secretion (**I**), ASC speck formation (**J**), pyroptosis (**K**) and K^+ efflux (**L**). After LPS priming and DSS treatment, BMDMs were incubated with BAPTA-AM in Ca^{2+}-free buffer for 40 min prior to ATP stimulation. The data are expressed as the mean ± SD. *$p < 0.05$, **$p < 0.01$, ***$p < 0.001$

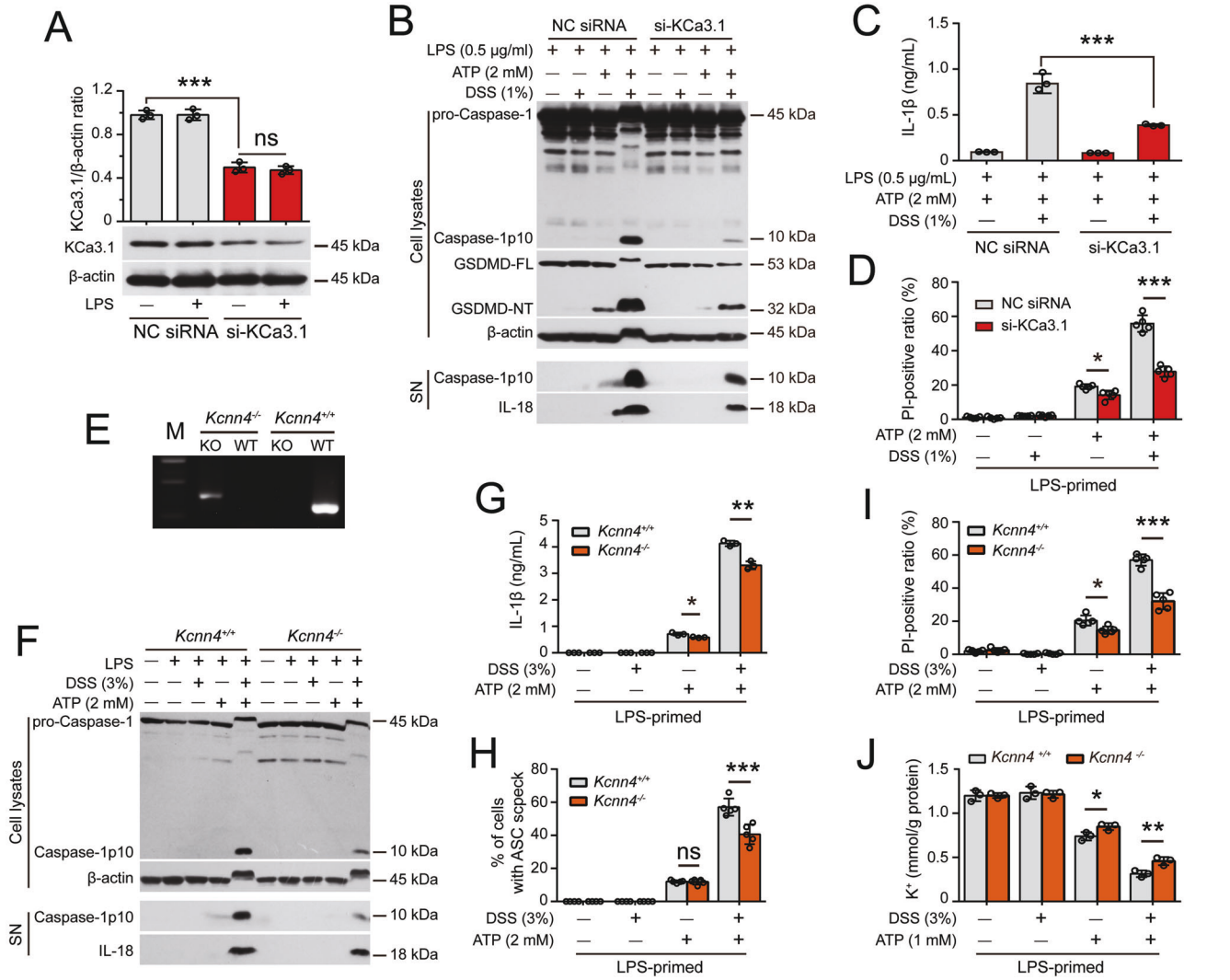

Fig. 6 *Kcnn4* (encoding KCa3.1) knockdown or knockout attenuates the DSS-induced increase in ATP-induced NLRP3 inflammasome activation. After being primed with LPS for 4 h, the cells were treated with DSS for 1 h followed by ATP stimulation. Western blot analysis was performed to examine the levels of the indicated proteins in culture supernatants (SN) and cell lysates. The formation of ASC specks was evaluated by immunofluorescence microscopy, and IL-1β levels in supernatants were measured with a CBA. Lytic cell death was assessed by PI and Hoechst 33342 staining. The K^+ concentration in cell lysates was measured by a potassium turbidimetric assay and normalized to the protein concentration in the homogenate (mmol/g protein). Specifically, the expression of KCa3.1 in J774A.1 cells was knocked down for 48 h with a specific siRNA (siRNA-KCa3.1). BMDMs from *Kcnn4*$^{-/-}$ mice and their littermates were used. **A** siRNA-KCa3.1 transfection decreased the expression of KCa3.1. The knockdown efficiency of siRNA-KCa3.1 was assessed by Western blotting, and band intensity was quantified with ImageJ software and normalized to β-actin. **B–D** Knockdown of KCa3.1 expression attenuated the DSS-induce enhancement of ATP-induced inflammasome activation (**B**), IL-1β release (**C**), and lytic cell death (**D**). **E** KCa3.1-deficient BMDMs were differentiated from *Kcnn4*$^{-/-}$ mice and genotyped by PCR. Representative electrophoretic results of the PCR analysis of *Kcnn4*$^{+/+}$ (320 bp) and *Kcnn4*$^{-/-}$ (417 bp) BMDMs with specific primers are shown. **F–J** KCa3.1 depletion attenuated the DSS-induced increase in ATP-induced inflammasome activation (**F**), IL-1β release (**G**), ASC speck formation (**H**), lytic cell death (**I**), and K^+ efflux (**J**). The data are expressed as the mean ± SD. ns not significant. *$p < 0.05$, **$p < 0.01$, ***$p < 0.001$

We also evaluated the time-dependent effects of TRAM-34 administration on colonic injury and inflammasome activation in the colon on Day 3 and Day 5 after DSS exposure. From Day 3 to Day 5, there was an increase in the severity of DSS-induced colitis, as evidenced by the loss of body weight, increase in DAI scores, shortening of the colon, and injury of colonic epithelial barriers (Fig. 8A–E). Interestingly, accompanying the increased severity of colitis, inflammasome activation in the colon was markedly increased, as revealed by the formation of ASC specks and the release of IL-1β, IL-18 and caspase-1p10, and these hallmarks were decreased by TRAM-34 administration (Fig. 8F–I), indicating that inflammasome activation and colitis induced by DSS are ongoing processes with the indispensable participation of KCa3.1.

Taken together, these results indicate that DSS-induced inflammasome activation correlates with the induction of colitis and that blocking KCa3.1 with the specific inhibitor TRAM-34 suppresses inflammasome activation in vivo and attenuates the severity of colitis, suggesting that the K^+ channel KCa3.1 is a critical mediator of the colitogenic activity of DSS.

KCa3.1 depletion mitigates DSS-induced colitis and decreases inflammasome activation

To further confirm the role of KCa3.1 in mediating DSS-induced inflammatory injuries in the colon, we examined whether knockout of *Kcnn4* (the gene encoding KCa3.1) has any effect on DSS-induced colitis in mice. Homozygotes of *Kcnn4*-ablated mice and

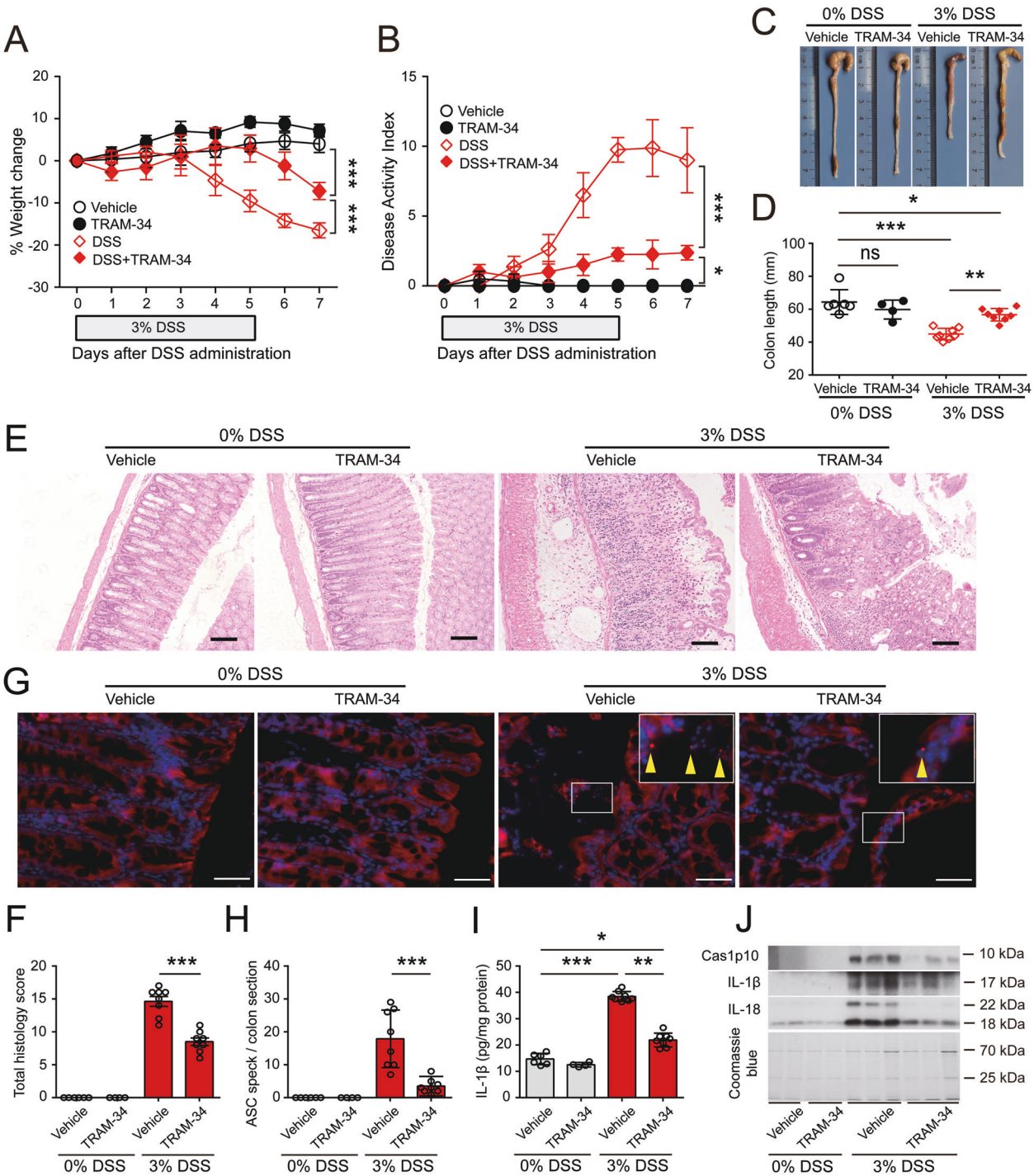

Fig. 7 Blockade of KCa3.1 by its inhibitor TRAM-34 mitigates DSS-induced injury and inflammasome activation in the colon in mice. DSS was dissolved in drinking water and fed *ad libitum*. After 5 days of DSS treatment, the mice were fed DSS-free normal drinking water and observed for another 2 days. TRAM-34 (40 mg/kg) or vehicle (peanut oil) was administered twice daily by intraperitoneal injection. **A**, **B** TRAM-34 administration protected mice from DSS-induced weight loss (**A**) and the increased in disease activity index (DAI) (**B**). **C**, **D** TRAM-34 reversed colonic shortening. Representative photographs of colons from vehicle- or TRAM-34-treated mice with or without DSS treatment are shown (**C**), and the length of the colon in each group was compared (**D**). **E**, **F** TRAM-34 administration attenuated tissue injury and inflammatory cell infiltration in the DSS-exposed colon. Representative H&E staining of colon sections from vehicle- or TRAM-34-treated mice with or without DSS treatment is shown (**E**). Scale bars, 100 μm. The histology score (the sum of the inflammation and injury histology scores) of each colon section was quantified and compared among the groups (**F**). **G**, **H** TRAM-34 suppressed ASC speck formation in the colons of DSS-treated mice. Frozen colon sections were prepared and incubated with anti-ASC antibodies (red) and counterstained with Hoechst 33342 (blue). Representative images of colonic ASC immunofluorescence in each group are shown (**G**). Arrowheads indicate ASC specks. Scale bars, 50 μm. The number of ASC specks in colon sections was quantified (**H**). **I**, **J** TRAM-34 reduced the release of caspase-1p10 (Cas1p10), IL-1β and IL-18 from DSS-treated colons. IL-1β levels in the supernatants of colon organ cultures were measured by a CBA and normalized to the total protein concentration (pg/mg protein). The precipitated proteins from the supernatants of colon organ cultures were analyzed by Western blotting. The data are expressed as the mean ± SD. ns, not significant. *$p < 0.05$, **$p < 0.01$, ***$p < 0.001$

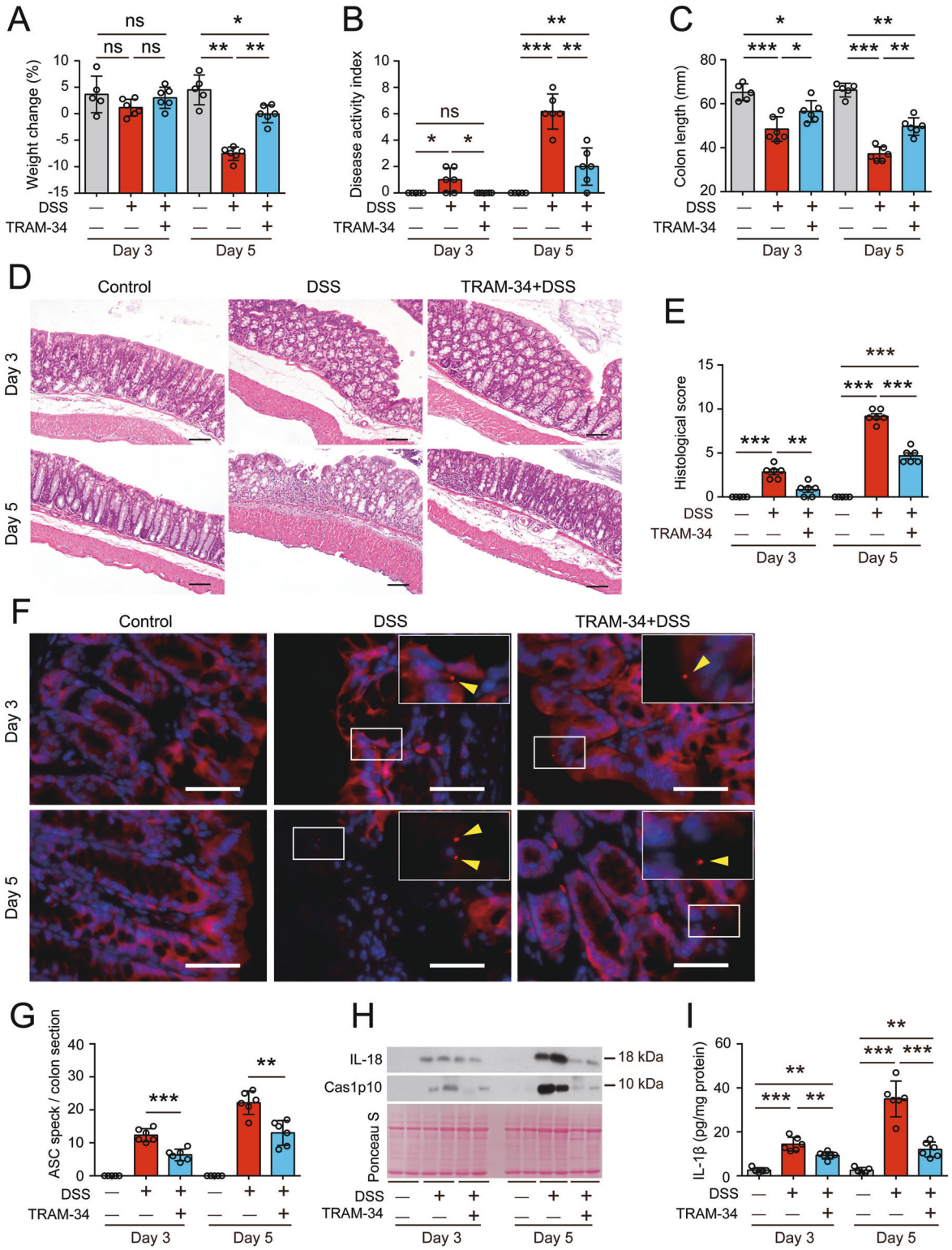

Fig. 8 The KCa3.1 inhibitor TRAM-34 inhibits inflammasome activation in the colon and reduces DSS-induced colitis-like symptoms in mice at early time points. The mice were administered DSS and TRAM-34 as shown in Fig. 5. After 3 days or 5 days of DSS treatment, the mice were sacrificed, and proximal segments of the colon were collected for colon organ cultures, while middle and distal segments were subjected to H&E staining or immunofluorescence microscopy. **A–C** Weight loss (**A**), DAI (**B**) and colon lengths (**C**) of vehicle- or TRAM-34-treated mice on Day 3 or Day 5 of DSS exposure. **D**, **E** TRAM-34 administration attenuated DSS-induced colon injury. Representative images of colonic sections (H&E.) are shown (**D**). Scale bars, 100 μm. The total histological score of each section was calculated and is shown as a histogram (**E**). **F**, **G** TRAM-34 administration suppressed ASC speck formation in the DSS-exposed colon. Representative images of colonic ASC immunofluorescence from vehicle- or TRAM-34-treated mice are shown (**F**). Arrowheads indicate ASC specks. Scale bars, 20 μm. The number of ASC specks in each colon section was quantified (**G**). **H**, **I** TRAM-34 reduced the DSS-induced release of caspase-1p10 (Cas1p10) (**H**), IL-18 (**H**) and IL-1β (**I**) from colon organ cultures. The data are expressed as the mean ± SD. $^{*}p < 0.05$, $^{**}p < 0.01$, $^{***}p < 0.001$

their WT littermates were confirmed by PCR genotyping (Fig. 9A). In the absence of DSS exposure, an increase in body weight was observed. In response to DSS exposure, the body weights of WT and *Kcnn4*$^{-/-}$ mice were decreased, whereas KCa3.1 depletion markedly reduced the body weight losses induced by DSS treatment (Fig. 9B). Consistently, mice with KCa3.1 depletion had significantly reduced DAI scores compared with their WT littermates (Fig. 9C). KCa3.1 deficiency did not impair the normal epithelium or crypts, nor did it cause any infiltration of inflammatory cells into the lamina propria (LP) of the colon. Notably, KCa3.1 depletion prevented DSS-induced colonic shortening in mice compared with WT littermates (Fig. 9D, E). Furthermore, histochemical analysis revealed that KCa3.1-deficient mice exhibited reductions in the number and size of ulcerative lesions, as well as decreased infiltration of inflammatory cells, and there was significantly reduced crypt loss compared with their WT littermates (Fig. 9F, G). Finally, we examined the effect of KCa3.1 depletion on inflammasome activation in the colon by measuring IL-1β levels in the supernatants of colon organ cultures and evaluating the formation of ASC specks in the colon. ASC specks were not observed in the untreated colon but were detected in the colon in response to DSS exposure (Fig. 9H). KCa3.1 depletion significantly reduced the formation of ASC specks in the colons of mice treated with DSS (Fig. 9I). Furthermore, although both the colons of WT (*Kcnn4*$^{+/+}$) and KCa3.1-depleted (*Kcnn4*$^{-/-}$) mice spontaneously released a small amount of IL-1β into colon organ culture supernatants in the absence of DSS exposure, the level of IL-1β released from *Kcnn4*$^{-/-}$ colons was lower than that released by *Kcnn4*$^{+/+}$ colons. After DSS treatment, the levels of IL-1β released by *Kcnn4*$^{-/-}$ and *Kcnn4*$^{+/+}$ colons were significantly increased, while the levels released from *Kcnn4*$^{-/-}$ colons were lower than those released from *Kcnn4*$^{+/+}$ colons (Fig. 9J). Consistently, the DSS-induced release of caspase-1p10 and IL-18 was decreased in the colons of *Kcnn4*$^{-/-}$ mice compared with those of their WT littermates (Fig. 9K). Taken together, these results further confirmed that KCa3.1 plays a critical role in DSS-induced ulcerative colitis by modulating inflammasome activation in the colon, suggesting that targeting KCa3.1 is an attractive therapeutic strategy for IBD.

DISCUSSION

The incidence and prevalence of IBD have increased in recent years, but the disease remains incurable despite substantial advances in both medical treatments and understanding its pathogenesis [7, 41, 42]. Although multiple IBD models have been developed, DSS-induced colitis remains one of the most frequently used models in IBD and anti-inflammatory drug research [9–11]. Thus, understanding the pathogenic mechanism(s) underlying DSS-induced colitis is still important. In this study, we found that DSS potentiates NLRP3 inflammasome activation induced by extracellular ATP or nigericin in vitro, and this effect is dependent on KCa3.1-mediated K^+ efflux. Pharmacological inhibition of KCa3.1 or genetic knockout of the *Kcnn4* gene (encoding KCa3.1) in mice inhibited the DSS-induced increase in inflammasome activation, thus mitigating the severity of colitis. Our data underscore the importance of KCa3.1 in mediating DSS-induced colitis, highlighting this channel as a potential therapeutic target for treating IBD, including CD and UC.

Although we have demonstrated that NLRP3 deficiency could ameliorate DSS-induced colitis in mice and reduce inflammasome assembly, we unexpectedly found that DSS alone was unable to directly trigger NLRP3 inflammasome assembly but instead potentiated ATP- or nigericin-induced NLRP3 activation. Several lines of evidence support this finding. First, DSS alone neither induced inflammasome assembly, as the cleavage of pro-caspase-1 and pro-IL-1β was not detectable, nor trigger pyroptotic cell death, as no GSDMD or GSDME cleavage was observed in LPS- or Pam3CSK4-primed macrophages. Second, in the presence of suboptimal doses of extracellular ATP or nigericin, DSS treatment robustly increased the abovementioned hallmarks of NLRP3 activation, indicating that DSS decreased the threshold of these stimuli to induce NLRP3 inflammasome activation. Third, the effect of DSS on inflammasome activation was fully abrogated by NLRP3 ablation or by MCC950, an NLRP3-specific inhibitor [37]. Fourth, DSS had minimal effects on the activation of NLRP6, NLRC4, and AIM2 inflammasomes, suggesting its preferable effect on NLRP3. Moreover, pyroptosis following NLRP3 inflammasome assembly was also suppressed by the caspase-1 inhibitor VX-765 or disulfiram, a GSDMD-NT inhibitor [43]. These data indicate that DSS potentiates but does not directly trigger NLRP3 inflammasome assembly in murine macrophages.

However, our data appear to be different from those of a previous study suggesting that DSS could induce NLRP3 inflammasome assembly in murine macrophages primed by LPS [19]. This difference may be due to differential experimental settings: the previous study treated cells with DSS after LPS priming for 24 h, and LPS may have been persistently present. If it was, the LPS could be internalized through receptor-mediated endocytosis alone or together with DSS and then released from endosomes to trigger caspase-11 activation [44, 45]. Activated caspase-11 subsequently generates GSDMD-NT to form plasma membrane pores that allow K^+ efflux, ultimately triggering the assembly of the NLRP3 inflammasome [26]. Under this condition, DSS might enhance such noncanonical NLRP3 inflammasome activation instead of directly triggering its assembly. However, in our study, we washed out LPS or Pam3CSK4 after priming for 4 h and then provided DSS stimulation, and the time period of DSS incubation was approximately 16 h.

Our in vitro experimental context of suboptimal ATP plus DSS may mimic the in vivo conditions in DSS-exposed colonic tissues. There are various bacteria in the colon, and it has been shown that both bacterial cells and host immune cells can release ATP to extracellular compartments [46, 47]. PAMPs derived from bacteria and ATP may initiate NLRP3 inflammasome assembly, which is further potentiated by DSS exposure. However, a low level of ATP produced by intestinal bacteria may not be sufficient to harm the colon, and DSS lowers the threshold at which ATP can induce inflammatory tissue injury.

It is worth noting that under normal physiological conditions, the intestinal epithelium is covered by a layer of mucins that protects the colon from bacterial invasion [48]. It is unclear how DSS can penetrate this mucus layer to reach epithelial cells and enter the lamina propria (LP), where macrophages and other immune cells reside. We suggest that DSS, which is a polymer with a high density of negative charges [11], may first bind to mucins and damage the mucus layer, leading to the exposure of colonic bacteria to epithelial cells. In support of this hypothesis, our results show that DSS can change the electrophoretic mobility of various proteins (e.g., Fig. 2A, B), indicating that DSS may nonspecifically bind to these proteins, thus impairing their normal structure. After the mucus layer is injured, colonic epithelial cells may be exposed to both DSS and bacterial-derived ATP or other PAMPs/DAMPs, leading to robust activation of the NLRP3 inflammasome and pyroptotic cell death, which is supported by our observation that ASC specks (indicating inflammasome assembly) formed in colonic epithelial cells and macrophages in the LP. Under these conditions, DSS might further penetrate the injured epithelial layer to enter the LP, where it can further augment NLRP3 inflammasome activation in macrophages, as well as other immune cells, in response to translocated bacteria or DAMPs (e.g., ATP) released from injured epithelial cells to propagate inflammatory cascades, culminating in severe colitis (Fig. S21).

Previous studies have shown that the major inflammasomes in IECs are NLRP6 and NLRP9b, while NLRP3 is predominantly expressed in gut macrophages [49–51]. However, the NLRP3

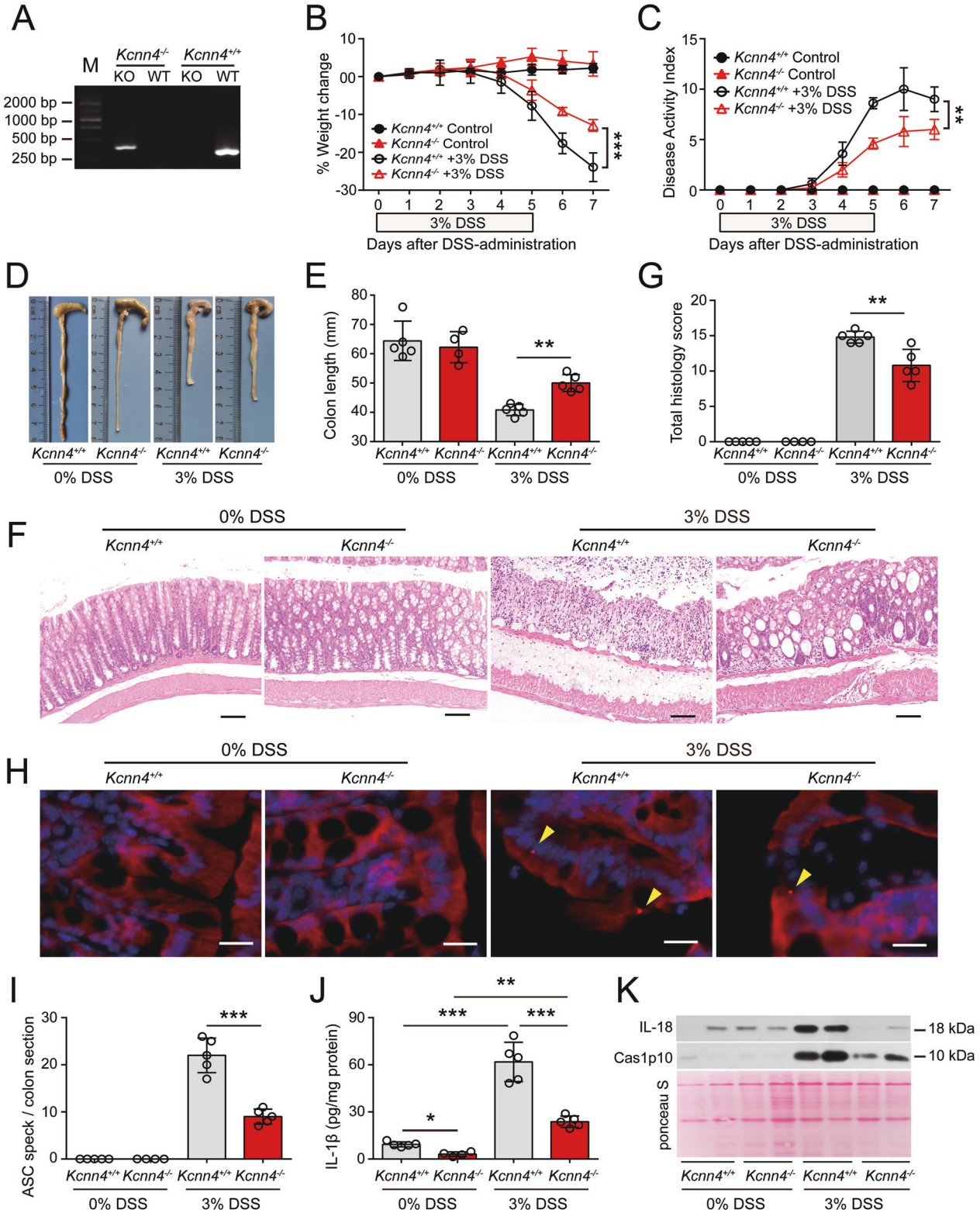

Fig. 9 KCa3.1 depletion alleviates DSS-induced injury and decreases inflammasome assembly in the colon. *Kcnn4*$^{-/-}$ and *Kcnn4*$^{+/+}$ littermates (9 weeks of age) were treated with drinking water containing 3% DSS for 5 days followed by DSS-free drinking water *ad libitum* for another two days. **A** Representative electrophoretic analysis of PCR products from *Kcnn4*$^{+/+}$ (320 bp) and *Kcnn4*$^{-/-}$ (417 bp) mice. **B–E** KCa3.1 depletion protected mice from DSS-induced weight loss (**B**), increases in the DAI (**C**), and shortening of the colon (**D**, **E**). **F**, **G** KCa3.1 deficiency attenuated colon injury and inflammatory cell infiltration in the DSS-exposed colon. Representative images of colonic sections (H&E.) are shown (**F**). Scale bars, 100 μm. The histology score of each colonic section was quantified (**G**). **H**, **I** KCa3.1 depletion suppressed ASC speck formation in the DSS-exposed colon. Representative images of colonic ASC immunofluorescence are shown (**H**). Arrowheads indicate ASC specks. Scale bars, 20 μm. The number of ASC specks in each colon section was quantified (**I**). **J**, **K** KCa3.1 depletion decreased the release of IL-1β (**J**), Caspase-1p10 (Cas1p10) and IL-18 (**K**) from DSS-treated colons. The data are expressed as the mean ± SD. *$p < 0.05$, **$p < 0.01$, ***$p < 0.001$

inflammasome has also been reported to be activated in IECs [52]. Consistent with the latter study, we not only observed an increase in NLRP3 protein levels in IECs from mice treated with DSS but also found ASC speck assembly in IECs, which was markedly reduced by NLRP3 depletion, indicating the involvement of NLRP3 in this process. Importantly, our in vitro data showed that NLRP6 inflammasome activation by its cognate ligand LTA-SA was unaffected by DSS, suggesting that this inflammasome plays a minor role in the DSS-induced increase in inflammasome assembly in the colon. In addition, because NLRP9b is activated by short double-stranded RNA stretches to form inflammasomes with ASC and caspase-1 [50], this effect might not be potentiated by the DSS-induced increase in K^+ efflux, even though we did not examine this possibility. However, in the DSS-induced colitis mouse model, the formation of ASC specks in NLRP3-depleted IECs suggest that other inflammasome sensors, such as NLRC4, AIM2, NLRP6 and NLRP9b, participate in ASC speck assembly in IECs in response to DSS exposure, but their exact roles remain to be clarified.

The major finding of our study is that the K^+ channel KCa3.1 plays a critical role in DSS-mediated potentiation of NLRP3 inflammasome assembly. In this study, we used a suboptimal dose of ATP or nigericin, at which only weak or undetectable activation of the NLRP3 inflammasome could be induced. However, in response to DSS exposure, NLRP3 inflammasome assembly was robustly augmented, as was K^+ efflux. Consistently, this augmented inflammasome assembly was completely abrogated by an increase in extracellular K^+ concentrations, suggesting that DSS-induced potentiation of NLRP3 assembly was dependent on K^+ channels that mediate K^+ efflux. Although previous studies have revealed that TWIK2 is the K^+ channel that mediates ATP-induced NLRP3 activation [28], we found that this channel played a minimal role in the increase in NLRP3 activation induced by DSS. In addition, inhibiting P2X7R (the ATP receptor) could block DSS-mediated potentiation of NLRP3 activation in the presence of ATP, but it had no effect on nigericin. Pannexin-1 was also unnecessary in this process. In addition to TWIK2, other K^+ channels, including calcium-activated K^+ channels (e.g., KCa3.1), voltage-gated K^+ channels, ATP-sensitive K^+ channels and inward rectifier K^+ channels, have been reported to mediate K^+ efflux under physiological and stress conditions [28, 39, 40]. In our study, however, blocking the latter three types of K^+ channels had minimal or partial effects on the DSS-induced augmentation, whereas inhibiting KCa3.1 markedly abrogated the DSS-induced increase in NLRP3 activation in response to ATP or nigericin. DSS promoted K^+ efflux, and pharmacologic blockade of KCa3.1 reversed this process. Importantly, in vivo pharmacologic blockade or genetic depletion of KCa3.1 markedly suppressed inflammasome assembly in the colon and reduced the severity of DSS-induced colitis. Thus, our results support a critical role of KCa3.1 in mediating the DSS-induced increase in NLRP3 activation in vitro and in vivo.

Low doses of ATP (e.g., 1-2 mM) can induce a rapid decrease in intracellular K^+ levels. Under such low ATP concentrations, the NLRP3 inflammasome was only weakly activated. Notably, this rapid decrease in intracellular K^+ levels was enhanced by DSS pretreatment and was effectively reversed by KCa3.1 blockade, suggesting the involvement of KCa3.1 in both processes. Previous studies also showed that low doses of ATP (<2 mM) induced weak release of IL-1β (indicating weak inflammasome activation), while a high dose of ATP (5 mM) triggered the robust release of IL-1β (indicating strong inflammasome activation), the latter of which depends on TWIK2 [28]. One explanation for this difference is that high ATP levels (5 mM, a supra-physiological concentration) may trigger the opening of TWIK2, while low ATP levels (2 mM or less) may predominantly induce the opening of KCa3.1. On the other hand, although a KCa3.1 inhibitor or *Kcnn4* siRNA knockdown markedly affected the DSS-induced increase in NLRP3 inflammasome assembly, *Kcnn4* knockout had only partial effects. This outcome suggests that other K^+ channels may compensate for KCa3.1 deficiency in vivo during the development or differentiation of macrophages, thereby weakening the effect of its depletion, which warrants further research.

The mechanism underlying DSS-mediated effects on KCa3.1 is unclear. DSS alone did not induce K^+ efflux, so its enhancing effects depended on other signals (e.g., ATP or nigericin) to activate the KCa3.1 channel. P2X7R is a cation-selective ion channel with relatively high Ca^{2+} permeability [53]. Thus, ATP-activated P2X7R may increase intracellular Ca^{2+} levels, which in turn leads to the opening of KCa3.1, a calcium-activated K^+ channel [54]. Indeed, blocking intracellular Ca^{2+} signaling with BAPTA-AM abrogated the DSS-induced increase in K^+ efflux and NLRP3 inflammasome activation, suggesting that calcium signaling is required to trigger the opening of the KCa3.1 channel in this process. However, ATP-induced intracellular Ca^{2+} signaling was not enhanced by DSS treatment, suggesting another mechanism of action. We hypothesized that DSS might act on the KCa3.1 channel directly: once activated, KCa3.1 undergoes conformational changes that may facilitate the binding of DSS to the channel, thus prolonging its opening and thereby elevating K^+ efflux. However, this hypothesis still needs further verification.

Although our in vitro studies were mainly performed on macrophages, we found that DSS potentiated inflammasome assembly both in colonic epithelial cells and in macrophages in the LP in vivo, suggesting that colonic epithelial cells also played an important role in mediating DSS-induced injury in the colon. These effects may be mediated by the K^+ channel KCa3.1 because KCa3.1 is expressed in macrophages and epithelial cells [55, 56]. It is possible that damage to the epithelial barrier of the colon occurs during the early stages after DSS exposure, followed by the entry of gut microorganisms and DSS into the LP, thereby leading to the robust propagation of inflammatory cascades and ulcerative colitis.

In addition to its expression in innate immune cells, KCa3.1 is also expressed in T and B cells, where it plays important roles in cell proliferation, differentiation, migration, and cytokine production [54, 57]. Our observations in mice are consistent with previous studies showing that the blockade of KCa3.1 significantly reduced the severity of colitis in DSS-induced IBD or $CD4^+$ T-cell-mediated mouse models of colitis [58, 59]. However, these previous studies provided evidence that the modulation of $CD4^+$ T-cell functions was responsible for the protective effects of KCa3.1 inhibition [58, 59]. Although a possible role of T cells in DSS-induced colitis cannot be excluded, our in vivo observations showed that macrophages but not T and B cells are the predominant immune cells recruited to the DSS-exposed colon and that a short period of DSS exposure (3 days) triggered inflammasome activation (revealed by ASC speck formation, caspase-1 autoprocessing and IL-1β secretion) in the colon, and these effects were significantly blocked by TRAM-34 administration. Our finding is consistent with previous findings that DSS-induced colitis did not involve T- or B-cell immunity, as DSS feeding resulted in very reproducible acute colitis in severe combined immunodeficient mice lacking functional T and B cells [60]. Thus, KCa3.1 may potentiate NLRP3 inflammasome assembly in macrophages and colonic epithelial cells in DSS-treated mice.

However, in contrast to our present study, one previous study showed that oral administration of the KCa3.1 inhibitor senicapoc had no significant effects on DSS-induced colitis in rats, although there was amelioration of endoscopic inflammation on Days 7 and 10 [61]. This discrepancy between a previous study and ours is likely due to differential experimental settings. Senicapoc (ICA-17043) has low bioavailability [62] and was given to rats via oral gavage in a previous study [61], whereas TRAM-34 has high bioavailability [63] and was administered to mice via intraperitoneal injection in our study.

Our data are consistent with previous studies showing the protective effects of NLRP3 suppression or depletion on DSS-

induced colitis [19–21]. Recent studies also support a critical role of NLRP3 in the pathogenesis of colitis in two animal models [64, 65]. On the other hand, it has been reported that NLRP3 depletion protected against DSS-induced colitis [25], which was mediated by the gut microbiota because cohousing NLRP3-depleted mice with WT mice largely abrogated this protective effect [33]. Indeed, other studies showed that NLRP3 depletion was able to alter the gut microbiota [51, 66]. However, it should be noted that the difference between the previous study [33] and ours may be due to different control mice: in the previous study, NLRP3-deficient (*Nlrp3*$^{-/-}$) and WT (*Nlrp3*$^{+/+}$) mice were provided separately by different institutions, and the *Nlrp3*$^{-/-}$ and *Nlrp3*$^{+/+}$ mice likely had other genetic background differences besides the gut microbiota [33], whereas in our study, *Nlrp3*$^{-/-}$ and their *Nlrp3*$^{+/+}$ littermates were produced by breeding heterozygote parents in house to minimize differences in their genetic background. In addition, we continuously cohoused *Nlrp3*$^{-/-}$ and sex-matched *Nlrp3*$^{+/+}$ littermates and separated them one week before DSS administration. The experimental settings of our study were designed to minimize the differences in the gut microbiota between *Nlrp3*$^{-/-}$ and *Nlrp3*$^{+/+}$ littermates before DSS administration but not affect the formation of the characteristic microbiota in *Nlrp3*$^{-/-}$ and *Nlrp3*$^{+/+}$ littermates after DSS treatment. Thus, our data suggest that *Nlrp3*$^{-/-}$ and *Nlrp3*$^{+/+}$ littermates with minimized differences in genetic background and cohousing conditions manifested distinct sensitivities to DSS-induced colitis, suggesting a pathogenic role of the NLRP3 inflammasome in this process.

Our data may have clinical implications, as an increase in the expression of KCa3.1 has been found to be associated with human rheumatoid arthritis, atherosclerosis and IBD [55, 67]. TRAM-34-mediated blockade of KCa3.1 confers protective effects in various mouse models of human diseases [58, 59, 68]. Further clinical investigations are therefore warranted.

In summary, we show that the potassium channel KCa3.1 plays a critical role in DSS-induced colitis in mice by potentiating NLRP3 inflammasome activation in colonic epithelial cells and macrophages in the LP. Inhibiting KCa3.1 can mitigate the severity of DSS-induced colitis in mice. Although it remains unclear how DSS promotes the function of KCa3.1 and further clinical research is still needed, our results suggest that targeting KCa3.1 may be leveraged as a new strategy for the treatment of human IBD and other related diseases.

REFERENCES

1. Graham DB, Xavier RJ. Pathway paradigms revealed from the genetics of inflammatory bowel disease. Nature. 2020;578:527–39.
2. Ng SC, Shi HY, Hamidi N, Underwood F, Tang W, Benchimol E, et al. Worldwide incidence and prevalence of inflammatory bowel disease in the 21st century: a systematic review of population-based studies. Lancet. 2017;390:2769–78.
3. Kobayashi T, Siegmund B, Le Berre C, Wei S, Ferrante M, Shen B, et al. Ulcerative colitis. Nat Rev Dis primers. 2020;6:74.
4. Atreya R, Neurath MF. Mechanisms of molecular resistance and predictors of response to biological therapy in inflammatory bowel disease. Lancet Gastroenterol Hepatol. 2018;3:790–802.
5. de Souza HSP, Fiocchi C, Iliopoulos D. The IBD interactome: an integrated view of aetiology, pathogenesis and therapy. Nat Rev Gastroenterol Hepatol. 2017;14:739–49.
6. Ananthakrishnan AN, Bernstein C, Iliopoulos D, Macpherson A, Neurath M, Ali R, et al. Environmental triggers in IBD: a review of progress and evidence. Nat Rev Gastroenterol Hepatol. 2018;15:39–49.
7. Chang JT. Pathophysiology of inflammatory bowel diseases. N Engl J Med. 2020;383:2652–64.
8. Kiesler P, Fuss IJ, Strober W. Experimental models of inflammatory bowel diseases. Cell Mol Gastroenterol Hepatol. 2015;1:154–70.
9. Okayasu I, Hatakeyama S, Yamada M, Ohkusa T, Inagaki Y, Nakaya R. A novel method in the induction of reliable experimental acute and chronic ulcerative colitis in mice. Gastroenterology. 1990;98:694–702.
10. Cooper HS, Murthy S, Shah R, Sedergran D. Clinicopathologic study of dextran sulfate sodium experimental murine colitis. Lab Invest. 1993;69:238–49.
11. Chassaing B, Aitken JD, Malleshappa M, Vijay-Kumar M. Dextran sulfate sodium (DSS)-induced colitis in mice. Curr Protoc Immunol. 2014;104:15.25.11–15.25.14.
12. Huang B, Chen Z, Geng L, Wang J, Liang H, Cao Y, et al. Mucosal profiling of pediatric-onset colitis and IBD reveals common pathogenics and therapeutic pathways. Cell. 2019;179:1160–76.
13. Pandey A, Shen C, Feng S, Man SM. Cell biology of inflammasome activation. Trends Cell Biol. 2021;31:924–39.
14. Broz P, Dixit VM. Inflammasomes: mechanism of assembly, regulation and signalling. Nat Rev Immunol. 2016;16:407–20.
15. Mangan MSJ, Olhava EJ, Roush WR, Seidel HM, Glick GD, Latz E. Targeting the NLRP3 inflammasome in inflammatory diseases. Nat Rev Drug Discov. 2018;17:688.
16. Li Y, Huang H, Liu B, Zhang Y, Pan X, Yu XY, et al. Inflammasomes as therapeutic targets in human diseases. Signal Transduct Target Ther. 2021;6:247.
17. Zhen Y & Zhang H, NLRP3 Inflammasome and inflammatory bowel disease. Front Immunol. 2019;10:276.
18. Villani AC, Lemire M, Fortin G, Louis E, Silverberg M, Collette C, et al. Common variants in the NLRP3 region contribute to Crohn's disease susceptibility. Nat Genet. 2009;41:71–76.
19. Bauer C, Duewell P, Mayer C, Lehr HA, Fitzgerald KA, Dauer M, et al. Colitis induced in mice with dextran sulfate sodium (DSS) is mediated by the NLRP3 inflammasome. Gut. 2010;59:1192–9.
20. Neudecker V, Haneklaus M, Jensen O, Khailova L, Masterson JC, Tye H, et al. Myeloid-derived miR-223 regulates intestinal inflammation via repression of the NLRP3 inflammasome. J Exp Med. 2017;214:1737–52.
21. Perera AP, Fernando R, Shinde T, Gundamaraju R, Southam B, Sohal SS, et al. MCC950, a specific small molecule inhibitor of NLRP3 inflammasome attenuates colonic inflammation in spontaneous colitis mice. Sci Rep. 2018;8:8618.
22. Cosin-Roger J, Simmen S, Melhem H, Atrott K, Frey-Wagner I, Hausmann M, et al. Hypoxia ameliorates intestinal inflammation through NLRP3/mTOR downregulation and autophagy activation. Nat Commun. 2017;8:98.
23. Mao L, Kitani A, Hiejima E, Montgomery-Recht K, Zhou W, Fuss I, et al. Bruton tyrosine kinase deficiency augments NLRP3 inflammasome activation and causes IL-1β-mediated colitis. J Clin Invest. 2020;130:1793–807.
24. Allen IC, TeKippe EM, Woodford RM, Uronis JM, Holl EK, Rogers AB, et al. The NLRP3 inflammasome functions as a negative regulator of tumorigenesis during colitis-associated cancer. J Exp Med. 2010;207:1045–56.
25. Zaki MH, Boyd KL, Vogel P, Kastan MB, Lamkanfi M, Kanneganti TD. The NLRP3 inflammasome protects against loss of epithelial integrity and mortality during experimental colitis. Immunity. 2010;32:379–91.
26. Rühl S, Broz P. Caspase-11 activates a canonical NLRP3 inflammasome by promoting K(+) efflux. Eur J Immunol. 2015;45:2927–36.
27. He Y, Zeng MY, Yang D, Motro B, Núñez G. NEK7 is an essential mediator of NLRP3 activation downstream of potassium efflux. Nature. 2016;530:354–7.
28. Di A, Xiong S, Ye Z, Malireddi RKS, Kometani S, Zhong M, et al. The TWIK2 potassium efflux channel in macrophages mediates NLRP3 inflammasome-induced inflammation. Immunity. 2018;49:56–65.
29. Ye J, Zeng B, Zhong M, Li H, Xu L, Shu J, et al. Scutellarin inhibits caspase-11 activation and pyroptosis in macrophages via regulating PKA signaling. Acta Pharm Sin B. 2021;11:112–26.
30. Zhong CS, Zeng B, Qiu JH, Xu LH, Zhong MY, Huang YT, et al. Gout-associated monosodium urate crystal-induced necrosis is independent of NLRP3 activity but can be suppressed by combined inhibitors for multiple signaling pathways. Acta Pharmacol Sin. 2021;43:1324–36.
31. Shu JX, Zhong C, Shi Z, Zeng B, Xu L, Ye J, et al. Berberine augments hypertrophy of colonic patches in mice with intraperitoneal bacterial infection. Int Immunopharmacol. 2021;90:107242.
32. Liu L, Li X. NLRP3 inflammasome in inflammatory bowel disease: friend or foe? Dig Dis Sci. 2017;62:2211–4.
33. Bauer C, Duewell P, Lehr H, Endres S, Schnurr M. Protective and aggravating effects of Nlrp3 inflammasome activation in IBD models: influence of genetic and environmental factors. Dig Dis. 2012;30:82–90.
34. Hara H, Seregin S, Yang D, Fukase K, Chamaillard M, Alnemri E, et al. The NLRP6 inflammasome recognizes lipoteichoic acid and regulates gram-positive pathogen infection. Cell. 2018;175:1651–64. e1614.
35. Zhao Y, Yang J, Shi J, Gong Y, Lu Q, Xu H, et al. The NLRC4 inflammasome receptors for bacterial flagellin and type III secretion apparatus. Nature. 2011;477:596–600.
36. Hornung V, Ablasser A, Charrel-Dennis M, Bauernfeind F, Horvath G, Caffrey D, et al. AIM2 recognizes cytosolic dsDNA and forms a caspase-1-activating inflammasome with ASC. Nature. 2009;458:514–8.
37. Coll RC, Robertson A, Chae J, Higgins S, Muñoz-Planillo R, Inserra M, et al. A small-molecule inhibitor of the NLRP3 inflammasome for the treatment of inflammatory diseases. Nat Med. 2015;21:248–55.

38. Groß CJ, Mishra R, Schneider KS, Médard G, Wettmarshausen J, Dittlein DC, et al. K(+) efflux-independent NLRP3 inflammasome activation by small molecules targeting mitochondria. Immunity. 2016;45:761–73.
39. Xu Z, Chen ZM, Wu X, Zhang L, Cao Y & Zhou P. Distinct molecular mechanisms underlying potassium efflux for NLRP3 inflammasome activation. Front Immunol. 2020;11:609441.
40. Dudem S, Sergeant GP, Thornbury KD & Hollywood MA. Calcium-activated K(+) Channels (K(Ca)) and therapeutic implications. Handb Exp Pharmacol. 2021;267:379–416.
41. Nielsen OH, New strategies for treatment of inflammatory bowel disease. Front Med (Lausanne). 2014;1:3.
42. Kaplan GG. The global burden of IBD: from 2015 to 2025. Nat Rev Gastroenterol Hepatol. 2015;12:720–7.
43. Hu JJ, Liu X, Xia S, Zhang Z, Zhang Y, Zhao J, et al. FDA-approved disulfiram inhibits pyroptosis by blocking gasdermin D pore formation. Nat Immunol. 2020;21:736–45.
44. Kayagaki N, Stowe IB, Lee BL, O'Rourke K, Anderson K, Warming S, et al. Caspase-11 cleaves gasdermin D for non-canonical inflammasome signalling. Nature. 2015;526:666–71.
45. Shi J, Zhao Y, Wang K, Shi X, Wang Y, Huang H, et al. Cleavage of GSDMD by inflammatory caspases determines pyroptotic cell death. Nature. 2015;526:660–5.
46. Wegiel B, Larsen R, Gallo D, Chin B, Harris C, Mannam P, et al. Macrophages sense and kill bacteria through carbon monoxide-dependent inflammasome activation. J Clin Invest. 2014;124:4926–40.
47. Piccini A, Carta S, Tassi S, Lasiglié D, Fossati G, Rubartelli A. ATP is released by monocytes stimulated with pathogen-sensing receptor ligands and induces IL-1beta and IL-18 secretion in an autocrine way. Proc Natl Acad Sci USA. 2008;105:8067–72.
48. Hansson GC. Mucins and the microbiome. Annu Rev Biochem. 2020;89:769–93.
49. Yin J, Sheng B, Yang K, Sun L, Xiao W, Yang H. The protective roles of NLRP6 in intestinal epithelial cells. Cell Prolif. 2019;52:e12555.
50. Zhu S, Ding S, Wang P, Wei Z, Pan W, Palm N, et al. Nlrp9b inflammasome restricts rotavirus infection in intestinal epithelial cells. Nature. 2017;546:667–70.
51. Yao X, Zhang C, Xing Y, Xue G, Zhang Q, Pan F, et al. Remodelling of the gut microbiota by hyperactive NLRP3 induces regulatory T cells to maintain homeostasis. Nat Commun. 2017;8:1896.
52. Song-Zhao G, Srinivasan N, Pott J, Baban D, Frankel G, Maloy K. Nlrp3 activation in the intestinal epithelium protects against a mucosal pathogen. Mucosal Immunol. 2014;7:763–74.
53. Valera S, Hussy N, Evans RJ, Adami N, North RA, Surprenant A, et al. A new class of ligand-gated ion channel defined by P2x receptor for extracellular ATP. Nature. 1994;371:516–9.
54. Feske S, Wulff H & Skolnik EY. Ion channels in innate and adaptive immunity. Annu Rev Immunol. 2015;33:291–353.
55. Toyama K, Wulff H, Chandy KG, Azam P, Raman G, Saito T, et al. The intermediate-conductance calcium-activated potassium channel KCa3.1 contributes to atherogenesis in mice and humans. J Clin Invest. 2008;118:3025–37.
56. Thompson-Vest N, Shimizu Y, Hunne B, Furness JB. The distribution of intermediate-conductance, calcium-activated, potassium (IK) channels in epithelial cells. J Anat. 2006;208:219–29.
57. Nguyen HM, Singh V, Pressly B, Jenkins DP, Wulff H, Yarov-Yarovoy V. Structural insights into the atomistic mechanisms of action of small molecule inhibitors targeting the KCa3.1 channel pore. Mol Pharmacol. 2017;91:392–402.
58. Ohya S, Fukuyo Y, Kito H, Shibaoka R, Matsui M, Niguma H, et al. Upregulation of KCa3.1 K(+) channel in mesenteric lymph node CD4(+) T lymphocytes from a mouse model of dextran sodium sulfate-induced inflammatory bowel disease. Am J Physiol Gastrointest Liver Physiol. 2014;306:G873–G885.
59. Di L, Srivastava S, Zhdanova O, Ding Y, Li Z, Wulff H, et al. Inhibition of the K+ channel KCa3.1 ameliorates T cell-mediated colitis. Proc Natl Acad Sci USA. 2010;107:1541–6.
60. Dieleman LA, Ridwan BU, Tennyson GS, Beagley KW, Bucy RP, Elson CO. Dextran sulfate sodium-induced colitis occurs in severe combined immunodeficient mice. Gastroenterology. 1994;107:1643–52.
61. Hansen L. The role of T cell potassium channels, KV1.3 and KCa3.1, in the inflammatory cascade in ulcerative colitis. Dan Med J. 2014;61:B4946.
62. Stocker J, De Franceschi L, McNaughton-Smith G, Corrocher R, Beuzard Y, Brugnara C. ICA-17043, a novel Gardos channel blocker, prevents sickled red blood cell dehydration in vitro and in vivo in SAD mice. Blood. 2003;101:2412–8.
63. Brown B, Pressley B, Wulff H. KCa3.1 channel modulators as potential therapeutic compounds for glioblastoma. Curr Neuropharmacol. 2018;16:618–26.
64. Liu L, Dong Y, Ye M, Jin S, Yang J, Joosse M, et al. The pathogenic role of NLRP3 inflammasome activation in inflammatory bowel diseases of both mice and humans. J Crohns Colitis. 2017;11:737–50.
65. Umiker B, Lee H, Cope J, Ajami N, Laine J, Fregeau C, et al. The NLRP3 inflammasome mediates DSS-induced intestinal inflammation in Nod2 knockout mice. Innate Immun. 2019;25:132–43.
66. Zhang Y, Huang R, Cheng M, Wang L, Chao J, Li J, et al. Gut microbiota from NLRP3-deficient mice ameliorates depressive-like behaviors by regulating astrocyte dysfunction via circHIPK2. Microbiome. 2019;7:116.
67. Friebel K, Schönherr R, Kinne RW, Kunisch E. Functional role of the KCa3.1 potassium channel in synovial fibroblasts from rheumatoid arthritis patients. J Cell Physiol. 2015;230:1677–88.
68. Vega G, Guequén A, Philp A, Gianotti A, Arzola L, Villalón M, et al. Lack of *Kcnn4* improves mucociliary clearance in muco-obstructive lung disease. JCI insight. 2020;5:e140076.

AUTHOR CONTRIBUTIONS

X.H, DO, QZ, and BZ designed the experiments. BZ, YH, SC, RX, LX, and JQ performed the experiments. BZ, FS, and SL acquired and analyzed the experimental data. BZ, DO, and XH prepared the manuscript. All authors have read and approved the final manuscript.

FUNDING

This work was supported by the National Natural Science Foundation of China (grant numbers 81773965 to X.H., 81873064 to DO, and 81673664 to QZ).

CONFLICT OF INTEREST

The authors declare no competing interests.

ADDITIONAL INFORMATION

Supplementary information The online version contains supplementary material available at https://doi.org/10.1038/s41423-022-00891-0.

Correspondence and requests for materials should be addressed to Qingbing Zha, Dongyun Ouyang or Xianhui He.